UNIVERSITY OF CALIFORNIA

Los Angeles

Glo1 deficit in mice results in age- and sex-dependent metabolic dysfunction

A thesis submitted in partial satisfaction of the requirements for the degree

Master of Science in Physiological Science

by

Ingrid Carolina Cely

2022

ABSTRACT OF THE THESIS

Glo1 deficit in mice results in age- and sex-dependent metabolic dysfunction

by

Ingrid Carolina Cely

Master of Science in Physiological Science

University of California, Los Angeles, 2022

Professor Xia Yang, Chair

Glyoxalase 1 (Glo1) is a critical enzyme responsible for the clearance of toxic dicarbonyls, which are precursors for advanced glycation end products (AGEs). *Glo1* has been implicated in the progression of cardiometabolic disorders such as obesity, insulin resistance, and coronary artery disease; however, the underlying mechanisms have yet to be elucidated. We characterized female and male *Glo1* heterozygous knockdown (*Glo1*$^{+/-}$) mice by evaluating metabolic phenotypes such as body weight, adiposity, glycemic control and plasma lipid profiles. We also evaluated atherosclerotic burden, levels of AGEs, and gene expression profiles across cardiometabolic tissues (liver, adipose, muscle and aorta) to identify pathway perturbations and potential regulatory genes. Partial loss of *Glo1* resulted in obesity, hyperglycemia, dyslipidemia and reorganization of lipid metabolism in metabolic tissues in an age and sex-dependent manner. *Glo1*$^{+/-}$ females displayed altered glycemic control and increased plasma triglycerides, which aligned with significant perturbations in genes involved in adipogenesis, PPARg and insulin signaling, and fatty acid metabolism pathways in liver and adipose tissues. Conversely, *Glo1*$^{+/-}$ males developed increased skeletal muscle mass and visceral adipose depots along

with changes in lipid metabolism pathways. For both cohorts, most phenotypes were manifested after 14 weeks of age indicating an age-dependent effect. Evaluation of methylglyoxal-derived AGEs demonstrated changes in only male skeletal muscle but not in female tissues, thus unlikely explaining the broad phenotypic and multitissue gene expression alterations in both sexes. Network analysis of the tissue-specific gene expression data identified transcription factors involved in cardiometabolic diseases such as Pparg (adipose), Hnf4a (liver), and Tcf21 (aorta) whose targets are altered in response to *Glo1* deficiency. Our results indicate that *Glo1* deficit perturbs metabolic health and metabolic pathways in a sex- and age-dependent manner without concordant changes in AGEs across metabolic tissues.

The thesis of Ingrid Carolina Cely is approved.

Aldons J. Lusis

Claudio Villanueva

Xia Yang, Committee Chair

University of California, Los Angeles

2022

DEDICATION

This thesis is dedicated to God, my parents, husband, mentors and close friends who have supported me along the way to make my academic dreams a reality.

TABLE OF CONTENTS

LIST OF FIGURES

ACKNOWLEDGEMENTS

I would like to express my utmost gratitude to Dr. Xia Yang for her guidance and mentorship throughout the years.

I would like to express my utmost appreciation to my committee members Dr. Aldons J. Lusis and Dr. Claudio Villanueva for their support and mentorship during my graduate studies.

I would like to extend my utmost gratitude to Dr. Joseph Esdin, my teaching associate mentor and supervisor for all of the support and guidance throughout my graduate studies. I would also like to acknowledge and thank the many laboratory members for their support and guidance with my project: Dr. In Sook Ahn, Dr. Graciel Diamante, Dr. Guanglin Zhang, Dr. Le Shu, Jonnby LaGuardia, Dr. Monty Blencowe and Dr. Richard Davis.

I would like to thank the UCLA IBP Department particularly Marisela Diaz-Vasquez for the continuous support, encouragement and guidance throughout my graduate studies.

INTRODUCTION

There is a global epidemic of obesity and related metabolic disorders such as cardiovascular disease (CVD) and type 2 diabetes (T2D). Despite current preventative and therapeutic strategies, prevalence remains on the rise and improved mapping of disease mechanisms may offer new biological insights and therapeutic targets. Glyoxalase 1 (Glo1) has recently been linked to obesity [1, 2], glycemic control [3], insulin sensitivity [4], aortic endothelial cell dysfunction [5], non-alcoholic fatty liver disease (NAFLD) [6], skeletal muscle dysfunction [7] and CVD [8] suggesting its importance in regulating metabolic health [9, 10]. The mechanisms underlying these associations, however, remain underexplored.

Glo 1 is part of the glyoxalase system, which is comprised of ubiquitous enzymes Glo1, Glyoxalase 2 (Glo2), and a catalytic amount of reduced glutathione (GSH) [11]. The glyoxalase system serves as a defense mechanism against the accumulation of reactive dicarbonyls such as methylglyoxal (MG), a cytotoxic byproduct of glycolysis. During glycolysis, MG is generated non-enzymatically by the spontaneous loss of a phosphate of an enediol intermediate, formed between the conversion of triphosphate isomers, glyceraldehyde-phosphate and dihydroxyacetone phosphate (DHAP). MG can also be generated by the removal of a phosphate group from DHAP by methylglyoxal synthase. [12]. Once generated, MG and GSH can spontaneously form a hemithioacetal, the substrate for Glo1. The enzyme-substrate complex can then generate S-D-Lactoylglutathione and this product is hydrolyzed by Glo2 to produce the final products, D-lactate and GSH. In essence, Glo1 is the main enzyme that initiates the process of converting a reactive

metabolite such as MG into D-lactate, a non-toxic and more stable product. The absence of glyoxalase detoxification can cause dicarbonyl stress due to the accumulation of MGs, which can react with DNA, lipids and amino acid residues of proteins. Dicarbonyl stress, due to abnormally elevated levels and decreased metabolism of MG, can be alleviated by compensatory enzymes such as aldehyde dehydrogenases (ALDH) and aldoketo reductases (AKR). ALDH and AKR can metabolize MG to pyruvate and hydroxyacetone [13], respectively to partially mitigate dicarbonyl stress.

MG readily reacts with arginine and lysine residues to irreversibly generate glycation end products (AGEs), making MG a major precursor for AGEs. The two most abundant MG-derived AGEs include *N*-(5-hydro-5-methyl-4-imidazolon-2-yl)-ornithine (MGH1) and carboxyethyl-lysine (CEL). The interaction between AGEs and their cell surface receptor RAGE plays a major role in the pathology of various diseases, including cancers, Alzheimer's Disease, non-alcoholic fatty liver disease, insulin resistance, diabetes and its complications including micro- and macrovascular disease, retinopathy, nephropathy and neuropathy [4, 14-17].

Despite the hypothesized involvement of the MG-AGE pathway in obesity and metabolic dysfunction, a thorough understanding of the causal role of *Glo1* and its associated mechanisms in obesity and metabolic dysfunction remains unclear. Therefore, we investigated the impact of *Glo1* on metabolism and obesity using a heterozygous *Glo1* knockdown (*Glo1*$^{+/-}$) mouse model expressing 45–65% decrease of enzymatic activity on a C57BL/6 background [18]. Investigating the mechanisms that lead to metabolic perturbations resulting from partial but not complete loss of

Glo1 activity is warranted due to its relevance to human health. Complete loss of *Glo1* rarely occurs in humans, yet Glo1 activity decreases with age [19]. Additionally, the effects of age and sex on *Glo1* functions have not been thoroughly examined. Furthermore, assessing the protective role of enzymes such as Akr1a1 and Aldh1a1 in metabolic tissues in the context of partial loss of *Glo1* remains to be explored.

In this study, we characterized sex- and age-dependent effects resulting from a partial loss of *Glo1* in mice on metabolic phenotypes such as body weight, adiposity, glycemic control and lipid profiles in mice overtime starting from 3 weeks of age up to ~30 week of age. MG-derived AGEs including MGH1 and CEL, as well as other players in the MG-AGE pathway including Rage, Aldh1a1 and Akr1a1 were quantified in major metabolic tissues such as liver, gonadal adipose and skeletal muscle. Results showed that female *Glo1*$^{+/-}$ mice produced broader phenotypes compared to male *Glo1*$^{+/-}$ mice, leading us to further assess and profile the transcriptome of liver, gonadal adipose and aorta to identify altered genes and pathways. Furthermore, integration of the tissue-specific transcriptomic signatures altered in female *Glo1*$^{+/-}$ mice with transcription factor networks and human genome-wide association studies provided additional mechanistic and clinical insights into the connection between *Glo1* and multiple human metabolic traits and diseases. Our findings strongly support an important age- and sex-dependent role for *Glo1* in mediating obesity and associated comorbidities through alterations of numerous metabolic pathways without major changes in AGEs or other components of the MG-AGE system.

METHODS

Heterozygous *Glo1* knockdown mice

The *Glo1*$^{+/-}$ mice were originally generated in Dr. Michael Brownlee's lab. In brief, short oligonucleotides with a target sequence to mouse *Glo1* in a hairpin sequence were subcloned into a lentiviral vector. The recombinant plasmids were used to generate lentiviral particles. shRNA lentivirus was injected into the perivitelline space of single-cell C57/B6 mouse embryos. After incubation for 4–6 hours, embryos were implanted into pseudo pregnant females and were carried to term. Mice whose genome contained a single copy of the insert were identified by Southern blotting and used to establish founder lines. Glo1 mRNA and protein levels were determined by quantitative PCR and Western blot analysis and further confirmed by measurement of Glo1 activity. Heterozygous offspring of the founder had a 45–65% decrease in tissue Glo1 activity, and these mice were used in all experiments [18] . *Glo1*$^{+/-}$ embryos were received as a gift from Dr. Abraham Palmer's lab and re-derived at the University of California, Los Angeles (UCLA) by the implantation of the embryo into a surrogate C57BL/6 female mouse. Offspring male *Glo1*$^{+/-}$ mice were selected for the purpose of breeding. Following this, multiple breeding pairs consisting of one female wildtype mouse and one male *Glo1*$^{+/-}$ mouse were set up to expand the mouse colony. All experiments on *Glo1*$^{+/-}$ mice and controls were conducted in accordance with the United States National Institutes of Health Guide for the Care and Use of Laboratory Animals and were approved by the UCLA Animal Research Committee.

Genotyping and husbandry

Genomic DNA was extracted from mouse ears (n=10-13 per sex) and analyzed by PCR using Kapa Mouse Genotyping Kit (Kapa Biosystems, Wilmington, MA, USA). Glo1 knockdown primers were as follows: forward (5'-GCTTCTCCCACAAGTCTGTG-3') and reverse (5'-GGTACAGTGCAGGGGAAAGA-3'). Gapdh primers served as the control and were as follows: forward (5'-AACTTTGGCATTGTGGAAGG-3') and reverse (5'-ACACATTGGGGGTAGGAACA-3'). Mice were provided with *ad libitum* standard chow diet (Newco Distributors Inc., Rancho Cucamonga, CA, USA) and water. Food and water intake were measured weekly to monitor caloric intake between groups.

Body weight and composition

Starting at 3-weeks of age, body weight was monitored weekly until the age of 28 weeks. Starting at 5-weeks of age, fat mass and lean muscle was monitored biweekly until the age of 27 weeks. Body weight was obtained by weighing mice on a scale and fat and lean mass data was obtained using nuclear magnetic resonance (NMR) (Brucker, Madison, WI, USA). Statistical analysis was done by 2-way ANOVA with repeated measures, followed by Bonferroni correction.

Intraperitoneal glucose tolerance test (IPGTT)

Mice underwent a glucose tolerance test at several time points of the experiment (5, 12, 23 and 33 weeks old). Mice were fasted overnight for 14 hours prior to IPGTT. Experiments were staggered to allow recovery in between invasive procedures. A 20% glucose solution (Sigma-Aldrich, St. Louis, MO, USA) was

prepared for intraperitoneal (IP) injection (2g of glucose per kg body mass). Blood samples (<5uL) for glucometer reading were obtained via mouse-tail incision. Blood glucose was measured at 15, 30, 60 and 120 minutes post glucose injection to test clearance of glucose.

Plasma lipid, glucose and insulin quantification

Quantification of blood plasma lipids, glucose and insulin was conducted at several time points of the experiment (7, 12 and 28 weeks of age). Prior to blood collection mice were fasted overnight for 14 hours. Fasted mice were anesthetized using isoflurane prior to blood collection by retro-orbital bleeding using a microcapillary tube. The collected blood was put into K2 EDTA tubes and placed on ice. The amount of blood obtained was 1% of the total body weight. Blood was then centrifuged at 1500g for 10 minutes and plasma was collected and stored in -80^{o}C. Plasma triglycerides (TG), total cholesterol (TC), high-density lipoprotein (HDL), glucose and insulin were analyzed by enzymatic colorimetric assays at UCLA GTM Mouse Transfer Core as previously described [20]. Very low-density lipoprotein cholesterol (VLDL) was calculated using the formula: VLDL= (TG/5).

Characterization of atherosclerotic lesions

Mice hearts were mounted with optimal cutting temperature (OCT) compound (VWR, Radnor, PA, USA) and placed in -80°C for histological purposes. Using a stereomicroscope, the heart was sliced longitudinally 10 m thick and fixed in 80% 2-propanol. The aortic sinus was stained with Oil red O (Abcam, Cambridge, MA, USA) and lesions were quantified. Cells were fixed in 10% formalin for 10 minutes,

rinsed 3 times in 1X PBS, placed in oil red O solution for 10 minutes, rinsed in tap water and counterstained with hematoxylin for 1 minute. An inverted phase-contrast microscope (Eclipse TE 300; Nikon Co., Tokyo, Japan) was used for identification of lesions.

Total RNA extraction, cDNA synthesis and qPCR

Mouse liver, gonadal adipose and skeletal muscle tissues were flash frozen in liquid nitrogen immediately after euthanasia. RNA extraction was performed using RNeasy Mini Kit (Qiagen, Germantown, MD, USA) following the manufacturer's instructions. RNA concentration was determined by Nanodrop ND-1000 Spectrophotometer (Thermo Fisher Scientific, Waltman, MA, USA). cDNA synthesis was performed using Applied Biosystems High-Capacity cDNA Reverse Transcription Kit (Thermo Fisher Scientific, Waltman, MA, USA). Expression of *Rage, Akr1a1, Aldh1a1, Lipin1, Acc1, Fasn, Elovl6, Scd1, Srebp1c, Dgat1 and Dgat2* was analyzed by qPCR using the Applied Biosystem Real-Time PCR Instrument (Thermo Fisher Scientific, Waltman, MA, USA) and SYBR Green Master Mix (Thermo Fisher Scientific, Waltman, MA, USA).

Protein extraction in metabolic tissues

Protein extraction of liver, gonadal adipose and skeletal muscle was performed according to the Abcam ELISA sample preparation guide on frozen tissue as follows: Approximately 50 mg of frozen liver and skeletal muscle tissue and 100mg of frozen gonadal adipose tissue were homogenized in the tissue extraction buffer which consists of 1% Triton X-100 (Thermo Fisher Scientific, Hudson, NH, USA), 100 mM Tris (pH 7.4), 150 mM NaCl, 1 mM EGTA, 1 mM EDTA, 0.5% sodium deoxycholate

and protease and phosphatase inhibitor cocktail (Abcam, Cambridge, MA, USA). The homogenized tissue was then centrifuged at 13000rpm for 20 minutes at 4°C and the supernatant containing the soluble protein extract was collected. Total protein concentration was evaluated by Bicinchoninic Acid (BCA) Protein Assay (Pierce, Rockford, IL, USA). Lysate was diluted to 2000ug/mL total protein for liver and skeletal muscle tissues and 500ug/mL total protein for gonadal adipose tissue in preparation for ELISA and western blotting.

ELISA quantification of AGEs

AGEs were quantified using the protein extracts from liver, gonadal adipose and skeletal muscle tissues. Quantification of MGH1 was performed using OxiSelect™ Methylglyoxal (MG) Competitive ELISA Kit (Cell Biolabs Inc., San Diego, CA, USA). Quantification of CEL was performed using OxiSelect™ N-epsilon-(Carboxyethyl) Lysine (CEL) Competitive ELISA (Cell Biolabs, San Diego, CA, USA). ELISA experiments were analyzed using a microplate reader (Biorad, Hercules, CA, USA) and Gen5 3.00 data analysis software.

Western blot analysis

Protein expression of Actin, Glo1, Camk2d and Rage was assessed in liver and kidney tissues of mice of 28 weeks of age. Western blot was performed using protein extracts from liver and kidney tissues.

Total RNA isolation, microarray profiling, and the identification of differentially expressed genes (DEGs)

Liver, gonadal adipose, and aorta tissues from 34-week old female mice were flash frozen in liquid nitrogen. About 10-15 mg tissue for liver and aorta and 30 mg for gonadal adipose tissue was homogenized and processed using RNeasy mini kit (QIAGEN GmbH, Hilden, Germany) for RNA isolation. RNA concentration was determined using Nanodrop (Thermo Fisher Scientific, MA, USA) and Bioanalyzer (Agilent Technologies, CA, USA). A total of 23 RNA samples passing quality control (RIN > 7.0) were sent to the UCLA Neuroscience Genomics Core facility for labeling and hybridization using the Illumina MouseRef-8 v2.0 array. There were 11 samples from C57/B6 WT control mice (3 samples/tissue, with the exception of aorta which had 2 samples), and 12 samples from *Glo1*$^{+/-}$ mice (3 samples/tissue). The gene expression data was deposited to Gene Expression Omnibus with accession number GSE118034. The Illumina array data were analyzed using the lumi Bioconductor package within R [21]. Data was transformed using the variance stabilization transformation, and then normalized it using the robust spline normalization. Differentially expressed genes (DEGs) between groups were identified using a linear model. False discovery rates (FDR) for the differential expression p-values were determined using the q-value Bioconductor package [22]. FDR<0.1 and p<0.01 were used as cutoffs to determine significant and suggestive DEGs, respectively, for downstream pathway, integrative genomics, and network analyses.

Functional annotation of *Glo1* deficiency DEGs

Glo1 deficiency DEGs identified from microarray analysis were annotated for their potential biological functions using canonical pathways or functional categories from various databases including Kyoto Encyclopedia of Genes and Genomes (KEGG) [23], BioCarta (http://www.biocarta.com/genes/index.asp), Reactome [24], and gene sets derived from Gene Ontology [25]. Fisher's exact test was performed to calculate the enrichment p-values for each pathway or functional category within the up- and down-regulated DEGs followed by multiple testing corrections using Storey's method [12].

Identification of enriched transcription factor downstream targets among Glo1 deficiency DEGs

To identify potential upstream regulators of *Glo1* deficiency DEGs, we assessed whether downstream target genes of transcription factors (TFs) were enriched in *Glo1* deficiency DEGs using the transcription factor networks for "adipose_tissue_adult", "aorta_adult" and "liver_adult" from the FANTOM5 database [26].The original connectivity of the FANTOM5 networks was too high, which violates the scale-free assumption of biological network topology and may lead to spurious results in subsequent analysis. Thus, we performed step-wise filtering by removing the networks edges with the lowest confidence score and recursively evaluated the scale-freeness of the resulting network. The removal process terminated as soon as the network reached boundary scale-freeness as defined by the criterion that at least 25% nodes have a degree (number of genes connected to the node) of 1. The downstream genes of each TF in the filtered network were

pooled as the target genes for that TF. TFs with more than 1000 targets were excluded. The enrichment for *Glo1* deficiency DEGs was then assessed using Fisher's exact test.

Assessing association between *Glo1* deficiency DEGs with human metabolic traits associated genetic signatures

To test whether there is a link between the genes identified from our study and human metabolic traits, we curated a total of 15 full sets of GWAS summary statistics in the public data repositories (i.e., disease association p-values of all the tested genetic risk variants in the form of single nucleotide polymorphisms, or SNPs) in existing large-scale GWAS of metabolic traits, including obesity (adult BMI [27], adult hip circumference [28], adult waist circumference [28], adult waist-hip ratio [28], T2D [29], CAD [30], glucose homeostasis traits HbA1c [31], fasting glucose [32], fasting insulin [32], the homeostatic model assessment for beta-cell function (HOMA-B) [33] and insulin resistance (HOMA-IR) [33], and lipid profiles (TC, TG, LDL, HDL) [34]. For each GWAS, we removed SNPs with a minor allele frequency < 0.05. For SNPs that are in linkage disequilibrium with $r^2 > 0.5$, only the SNP with the strongest disease association was kept. We then used a Market Set Enrichment Analysis (MSEA) to determine whether the genes affected in our *Glo1*$^{+/-}$ animal model were also enriched for SNPs that demonstrated evidence for disease association in humans. MSEA assesses whether a defined group of genes (in this study, DEGs) shows enrichment of disease-associated SNPs compared to random chance [35]. GWAS reported SNPs within the 50kb up/down-stream chromosomal distance of a gene was mapped to the corresponding gene. For the list of markers

mapped to each gene-set, MSEA tested the enrichment of markers for disease association using a chi-square like statistic:, where n denotes the number of quantile points (we used ten quantile points ranging from the top 50% to the top 99.9% based on the rank of p-values), O and E denote the observed and expected counts of positive findings (i.e. signals above the quantile point), and $\kappa = 1$ is a stability parameter to reduce artefacts from low expected counts for small gene sets. The varying quantile thresholds allow the statistic to be adoptable to studies of varying sample size and statistical power. The null background was estimated by permuting gene labels to generate random gene sets matching the gene number of each gene set, while preserving the assignment of markers to genes. For each gene set, 10000 permuted gene sets were generated and enrichment p-values were determined from a Gaussian distribution approximated using the enrichment statistics from the 10000 permutations and the statistics of the gene sets. Finally, Benjamini-Hochberg FDR was estimated across all modules tested for each GWAS. MSEA has been used to test the potential causal role of sets of genes of interest to human diseases [36-39].

RESULTS

Glo1 deficiency affects body composition

To investigate the effects of *Glo1* deficiency and determine when phenotypes would manifest **(Figure 1A; overview of experimental design)**, body weight was monitored weekly **(Figure 1B)** starting at weaning age until 28 weeks of age (n=10-13/group). Fat and muscle mass were monitored biweekly starting at 5

weeks of age and monitored until 27 weeks of age **(Figure 1C-1D)**. Compared to WT counterparts, female *Glo1*$^{+/-}$ mice started exhibiting significantly higher body weight at 17 weeks and male *Glo1*$^{+/-}$ mice at 15 weeks and continued this trend until 28 weeks of age **(Figure 1B; 2-way ANOVA with repeated measures)**. Female and male *Glo1*$^{+/-}$ mice both showed significantly increased fat mass at 15 weeks and this continued throughout their 28-week lifespan **(Figure 1C)**. Interestingly, male *Glo1*$^{+/-}$ mice showed significantly increased muscle mass at 11 weeks of age until 28 weeks (week 15 not significant) compared to control mice, whereas no change in muscle mass was observed between female groups at any point in time **(Figure 1D)**. Lastly, both female and male *Glo1*$^{+/-}$ mice demonstrated significantly increased adiposity **(Figure 1E)** at 15 weeks and throughout their lifespan, compared to their corresponding controls. Cardiometabolic tissue weights including liver, kidney, heart, skeletal muscle weight and fat pads (gonadal, subcutaneous, retroperitoneal, mesenteric and perirenal adipose) were also compared between groups at 28 weeks of age **(Figure 1F-1O)**. Female *Glo1*$^{+/-}$ tissue weights **(Figure 1F-1J)** showed a significant increase in kidney and subcutaneous adipose weight compared to controls **(Figure 1G, 1J)**. Male *Glo1*$^{+/-}$ tissue weights **(Figure 1K-1O)** showed a significantly increased liver, kidney, heart, gonadal, retroperitoneal and mesenteric adipose tissues compared to controls **(Figure 1K-1M, 1O)**. Although skeletal muscle tissue weights remained unaltered between male groups **(Figure 1N)**, *Glo1*$^{+/-}$ male muscle mass determined by NMR showed a significant increase compared to controls **(Figure 1D, right)**. Skeletal muscle tissue was removed from the vastus lateralis from bilateral hindlegs, whereas, muscle mass determined by NMR data accounted for

whole body muscle mass, likely explaining why increased skeletal muscle was not observed at the time of tissue harvesting. Together, these results suggest that decreased *Glo1* expression results in obesity post-developmentally in both female and male in mice.

Glo1 deficiency induces glucose intolerance in female but not male mice

To assess the impact of *Glo1* deficiency on glucose tolerance over time, we performed IPGTT experiments on 14-hour fasted mice at 7, 12, 23, 28 and 33 weeks of age **(Figure 2A-2C, 2E-2G)**. Additional mice for both sexes in each group (n=5/group) were exempt from the 28-week endpoint to further assess glycemic phenotypes at the 33-week endpoint **(Figure 2D, 2H).** We observed significantly increased glucose AUC in female $Glo1^{+/-}$ mice at 23 weeks (n=8/group) and 33 weeks (n=5/group) compared to WT **(Figure 2I)** but no differences in male $Glo1^{+/-}$ mice **(Figure 2L)** suggesting impaired ability to clear elevated glucose in blood in female $Glo1^{+/-}$ mice in an age-dependent manner. A possible explanation for impaired glucose clearance in female $Glo1^{+/-}$ mice but not in male $Glo1^{+/-}$ mice may involve the increased skeletal muscle in males which contributes to blood glucose homeostasis. Moreover, blood plasma glucose and insulin levels were also measured to determine potential changes in blood glucose and insulin levels in response to *Glo1* deficiency overtime **(Figure 2J-2K, 2M-2N)**. Fasted females showed no difference between cohorts when comparing plasma glucose **(Figure 2J)** or plasma insulin **(Figure 2K)**. In the fasted male cohorts, we observed significantly decreased plasma glucose levels at 12 weeks of age for male $Glo1^{+/-}$ mice compared to controls **(Figure 2M)** without any differences observed in

plasma insulin levels **(Figure 2N)**. This data demonstrates that *Glo1* deficiency results in the development of glucose intolerance in female but not male mice.

Glo1 deficiency results in dyslipidemia in a sex-dependent manner

To assess the impact of Glo1 deficiency on lipid phenotypes over time, we measured TG, TC, HDL and VLDL from blood plasma after fasting overnight for 14 hours in both sexes **(Figure 3A-3N)**. Changes in lipid profile, characterized by significantly elevated TG **(Figure 3A)** and VLDL **(Figure 3G)** levels, was observed in female *Glo1*$^{+/-}$ mice at 28 weeks compared to WT counterparts. Changes in TC, UC, FFA, HDL and LDL were not observed between female groups **(Figure 3B-3F)**. For male cohorts surprisingly, male *Glo1*$^{+/-}$ mice revealed hypolipidemia, a contrasting lipid phenotype to female *Glo1*$^{+/-}$ mice, characterized by significantly decreased TG **(Figure 3H)** at 28 weeks, decreased TC **(Figure 3I)** at 12 and 28 weeks and decreased HDL **(Figure 3L)** at 12 and 28 weeks of age. There were no changes observed in UC **(Figure 3J)** , FFA **(Figure 3K)**, LDL **(Figure 3M)** and VLDL **(Figure 3N)** in blood plasma between male groups at any given point. While both female and male *Glo1*$^{+/-}$ mice show evidence for dyslipidemia at 28 weeks, the metabolic phenotypes manifested are sex-dependent.

Long-term *Glo1* deficiency does not result in atherosclerosis

Due to the obesity prone characteristics observed in *Glo1*$^{+/-}$ mice and the known link between obesity and atherosclerosis, we sought to investigate if *Glo1* deficiency played a role in the development of cardiometabolic phenotypes. To assess if *Glo1* deficiency resulted in cardiometabolic phenotypes, we evaluated the occurrence of

atherosclerotic lesions in the aortic arch using red oil O staining. Our results showed no evidence for aortic lesions in 34-week-old female and male *Glo1*$^{+/-}$ mice compared to controls (n=4-5/group, data not shown) , suggesting that partial loss of *Glo1* alone does not induce atherosclerosis in mice. These findings align with numerous studies reporting the natural resistance of atherosclerosis in B6 mice. The mice used in our studies were not crossed with atherosclerosis-prone backgrounds such as *ApoE*$^{-/-}$ or *Ldlr*$^{-/-}$, nor were they challenged with atherogenic diets. These results suggest that *Glo1* deficiency in both female and male mice promotes obesity prone phenotypes without perpetuating cardiometabolic risk factors.

Glo1 deficiency perturbs lipid pathways in metabolic tissues

To assess whether lipid pathways were altered in parallel to the lipid phenotypes observed in *Glo1* deficient mice, we assessed select fatty acid and triglyceride metabolism genes (*Lipin1, Acc1, Fasn, Elovl6, Scd1, Srebp1c, Dgat1 and Dgat2)* in liver, gonadal adipose and skeletal muscle in mice of both sexes using qPCR **(Figure 4)**. Our findings show both sex-independent changes as well as sex-dependent changes in lipid genes across different tissues **(Figure 4A)**. Among the sex-independent changes in *Glo1* deficient mice, we observed decreased expression of *Acc1*, the gene encoding the rate-limiting enzyme in fatty acid synthesis, across all tissues; increased expression of *Fasn*, the gene encoding a key enzyme in *de novo* lipogenesis, in gonadal adipose tissue; decreased *Lipin1*, the gene encoding one of three enzymes that catalyze the conversion of phosphatidate to diacylglycerol, in liver and gonadal adipose tissue. Among the sex-dependent

changes is decreased *Srebp1c*, a transcription factor known to target *Fasn* and increase lipid production, in female liver but unaltered in any male tissues. It is interesting to note that nearly all lipid synthesis genes in the liver in female *Glo1*$^{+/-}$ mice were significantly downregulated, while in male *Glo1*$^{+/-}$ mice, only *Lipin1* and *Acc1* were significantly downregulated in the liver. *Dgat1* and *Dgat2,* which directly catalyze the formation of triglycerides, were upregulated in female gonadal adipose tissue but not male gonadal adipose despite the increased fat mass in both *Glo1* deficient groups. Lastly, male *Glo1*$^{+/-}$ mice showed significantly upregulated *Scd1* in liver and skeletal muscle. *Scd1* encodes Scd1, the rate-limiting enzyme in the biosynthesis of monounsaturated fatty acids, known to play a role in protecting against adiposity and increase insulin sensitivity when knocked out in mice [40]. These results indicate sex-specific alterations of the lipid metabolic pathways across tissues that may underly sex differences in metabolic phenotypes in *Glo1*$^{+/-}$ mice **(Figure 4B)**.

AGE levels in metabolic tissues may not explain phenotypic changes in *Glo1* deficient mice

AGEs have been implicated as an important mediator of Glo1-induced metabolic disorders[1, 4, 10]. Accumulated MG, in part due to a dysfunctional glyoxalase system and unavailability of compensatory enzymes, can readily react with proteins to generate AGEs **(Figure 5A).** However, the role of MG-derived AGEs in promoting obesity prone phenotypes in the context of partial loss of *Glo1* in mice is not clearly known. To investigate the role of AGEs in promoting sex and age dependent phenotypes and lipid pathway reprogramming observed in *Glo1*$^{+/-}$ mice, we

assessed metabolic tissues by ELISA, qPCR and microarray **(Figure 5B-5F).** MGH1 and CEL are both MG-derived AGEs that bind to the AGE receptor, RAGE. MGH1 and CEL are two of the most abundant AGEs although, CEL is less abundant compared to MGH1, making both compounds a suitable choice for AGE analysis [41-43]. MGH1 (n=6-8/group) and CEL (n=5/group) were quantified in the liver, gonadal adipose and skeletal muscle in both sexes **(Figure 5B)**. In *Glo1*$^{+/-}$ females, there was no significant difference in MGH1 and CEL levels compared to controls across any of the tissues analyzed **(Figure 5B)**. In contrast, only MGH1 was significantly elevated in male *Glo1*$^{+/-}$ skeletal muscle compared to controls while there was no difference in CEL between male groups in any tissue **(Figure 5B)**. To elucidate how unaltered levels of AGEs in metabolic tissues correspond to changes in the receptor for AGEs, we assessed gene expression of *Ager*, the gene that encodes Rage, in liver, gonadal adipose and skeletal muscle tissues by qPCR **(Figure 5C)**. Our results show that Rage was significantly decreased in skeletal muscle independently of sex in *Glo1* deficient mice **(Figure 5C)**. In addition, Rage was also significantly decreased in the liver but specifically in male *Glo1* deficient mice compared to their corresponding controls while Rage levels in gonadal adipose tissues for both sexes remained unaltered between groups **(Figure 5C)**. Initially, these findings appeared to be at odds with our previous assessment of AGEs in skeletal muscle tissues, particularly in male *Glo1*$^{+/-}$ mice, in which significantly elevated MGH1 was observed compared to controls. These unexpected findings were based on our knowledge of ligand-receptor interaction in which increased ligands result in increased receptor for that ligand. However, it has been reported that RAGE expression is found to be increasingly abundant in lung and skin and virtually absent in other tissues, notably

skeletal muscle in healthy adults. Moreover, protein quantification of Rage was assessed in *Glo1*$^{+/-}$ mice at 28 weeks of age (n=4/group) in liver and kidney using different antibody concentrations (1:1000 and 1:500 antibody) by western blot. Similarly, our results showed no significant changes in Rage protein between group in any sex in liver and kidney, further validations our previous findings. Overall, our results seem to suggest that MG-derived AGEs may not contribute to the alterations observed in lipid metabolism genes in liver, gonadal adipose and skeletal muscle tissues. Furthermore, since AGEs results from our study cannot explain the changes observed in lipid metabolism genes from the same metabolic tissues, the source of obesity prone phenotypes in *Glo1* deficient mice still remains to be investigated.

We next aimed to understand the role of compensatory enzymes in aiding in the prevention of AGE accumulation as observed in our previous findings **(Figure 5B)**. While detoxification of MG primarily occurs via the glyoxalase system and initiated by Glo1, compensatory enzymes such as Akr and Aldh are also involved in the clearance of MG to attenuate the formation of AGEs [13] **(Figure 5A).** Yet the extent of compensatory enzymes in aiding in the prevention of MG-derived AGEs in the context of partial loss of *Glo1* is not clearly known. To investigate the role of compensatory enzymes in promoting sex and age dependent phenotypes and lipid pathway reprogramming observed in *Glo1*$^{+/-}$ mice, we assessed gene expression of *Akr1a1* and *Aldh1a1* in liver, gonadal adipose and skeletal muscle tissues **(Figure 5C)**. *Ark1a1* was significantly upregulated in male *Glo1*$^{+/-}$ skeletal muscle without any changes in the other tissues. *Aldh1a1* was also significantly upregulated in male *Glo1*$^{+/-}$ liver and female *Glo1*$^{+/-}$ skeletal muscle. Neither of compensatory enzymes were upregulated in gonadal adipose tissue, possibly indicating a lack of protection

against MG in adipose tissue. To further investigate the specific isoforms of Akr and Aldh involved in metabolizing MG, we looked at gene expression changes in microarray data in 34-week old female *Glo1*$^{+/-}$ mice **(Figure 5D-5E)**. Female mice were further assessed over male mice due to prominent metabolic abnormalities observed in phenotypes including obesity, impaired glucose metabolism and elevated plasma lipids. Microarray analysis from liver, gonadal adipose, kidney and aorta tissues from female mice revealed significantly upregulated and downregulated gene expression of both compensatory enzymes across all tissues **(Figure 5D)**. Notably, kidney tissue of female *Glo1*$^{+/-}$ mice revealed several significantly upregulated gene expression for both Akr and Aldh. Among these upregulated genes is *Akr1b3*, known to regulate the accumulation of both AGEs and Rage. In gonadal adipose tissue, several genes were significantly downregulated further indicating reduced protection against MG. The aorta gene expression data trended upwards despite data not being statistically significant. Lastly, GSEA plots of a curated DEG list from female microarray data showed an insignificant enrichment score of the gene expression analyzed **(Figure 5E)**.

Together these results suggest that despite partial loss of *Glo1,* mice maintain elevated protection against MG due to specific compensatory enzyme availability. Overall, our results suggest that the metabolic disturbance induced by *Glo1* deficiency in mice may not be solely mediated through changes in AGEs.

Glo1 **deficiency leads to tissue-specific transcriptomic alterations in multiple metabolic tissues**

Due to the broader phenotypes observed in the females, including increased body weight, fat mass, plasma lipids and disrupted glucose metabolism, global transcriptomic changes in female *Glo1* deficient mice were analyzed. In addition, with the unaltered skeletal muscle phenotypes observed in female *Glo1*$^{+/-}$ mice, we selected the aorta as a replacement to assess global transcriptomic changes in addition to liver and gonadal adipose. Female mice are also more prone to atherosclerosis than male mice further supporting our choice to study the aorta and the effects of *Glo1* deficiency. Also, to ensure signaling related to atherosclerosis would be detected, we assessed female *Glo1*$^{+/-}$ mice at 34 weeks of age, which is a later age compared to when the previous phenotypes were observed.

To uncover the molecular basis of the obesity and glucose intolerance in female mice, we profiled the transcriptome of metabolic tissues including gonadal adipose, aorta, and liver in 34-week old female mice. Expression profiling showed that *Glo1* expression was lowered by 46% in adipose ($p = 3.2e-3$), 55% in aorta ($p = 1.3e-3$), and 46% in liver ($p = 1.5e-4$), confirming the Glo1 deficiency in these animals. At FDR < 0.1, a total of 96, 168, 347 differentially expressed genes (DEGs) were found in adipose tissue, aorta, and liver, respectively **(Figure 6A; Table 1)**, suggesting large-scale transcriptomic alterations in *Glo1*$^{+/-}$ mice.

Glo1 deficiency gene signatures exhibited strong tissue specificity when we compared the DEGs across tissues **(Figure 6A)**. For adipose tissue, aorta and liver, 80.2%, 88.7% and 92.5% of signatures were unique for the respective tissue. Two genes were found to be overlapped and consistently down-regulated in all three tissues, including *Nqo2* (N-Ribosyldihydronicotinamide: Quinone Reductase) and *Tuba1a* (Tubulin Alpha 1a). *Nqo2* is an antioxidant gene that may protect against

diabetes-induced endothelial dysfunction [48], whereas *Tuba1a* is the gene responsible for producing cytoskeleton protein tubulin, a known target for glyoxalase system defect [5]. The consistent alterations in these genes suggest that *Glo1* deficiency promotes oxidative stress and damage to cellular structure.

Glo1 deficiency perturbs metabolic pathways systemically

To determine the pathways affected by *Glo1* deficiency in each tissue, we performed pathway enrichment analysis of the tissue-specific DEGs from female *Glo1*$^{+/-}$ mice **(Figure 6B)**. We found an enrichment of genes involved in diacylglycerol (DAG) metabolism, glucose metabolism, and cytokine signaling in adipose, which is consistent with the glucose intolerance phenotype in *Glo1*$^{+/-}$ female mice [44-47]. Additionally, dysregulation in pathways related to lipid homeostasis were consistently captured across aorta (peroxisomal lipid metabolism, triglyceride biosynthesis) and liver (fatty acid metabolism, PPAR signaling, steroid hormone biosynthesis, biological oxidation). These results suggest that *Glo1* deficiency has a systemic impact on metabolic pathways across tissues. Furthermore, we investigated the expression patterns of DEGs involved in adipocyte differentiation, adipocytokine, insulin signaling and fatty acid/triglyceride biosynthesis in adipose tissue **(Figure 6C)**. We observed alterations in key genes involved in these processes such as *Elovl6, Fasn, Lep, Ppargc1a, Mapk9*, and *Pck1*. These transcriptomic changes in female mice may underlie the obesity, hyperlipidemia, and glucose intolerance phenotypes observed in female *Glo1*$^{+/-}$ mice.

Identification of transcription factor (TF) hotspots underlying *Glo1* deficiency signatures

To better understand how *Glo1* deficiency leads to the perturbations of DEGs in individual tissues, we explored transcription factors (TF) that may mediate the gene expression changes induced by *Glo1* knockdown. We leveraged the FANTOM5 TF networks and evaluated the enrichment for Glo1 deficiency signatures in local TF subnetworks. Interestingly PPARG, the master regulator of adipogenesis, is among the top perturbed adipose TF hotspots, as its target genes are highly enriched among the adipose DEGs **(Table 1)**. Moreover, several other TFs implicated in adipogenesis were also highly ranked in adipose TF hotspots, including KLF12 [49], ATF3 [50] and GATA5 [51]. These findings align with the increased adiposity in female *Glo1*$^{+/-}$ mice. In aorta, we identified perturbations in a number of TFs involved in circadian clock regulation (ARNTL, BHLHE40 and BHLHE41) [52], endothelial cell inflammation (TFEB) [53], and TCF21, a major coronary artery disease gene [54]. In the liver, several members of the hepatocyte nuclear factor (HNF) and forkhead box (FOX) gene families were captured as TF perturbation hotspots. These TFs exhibit significant regulatory roles during liver development and control key liver functions in adulthood [55], indicating the potential of Glo1 to alter a wide spectrum of physiological activities in the liver. These tissue-specific TFs likely mediate the effects of *Glo1* deficiency on the molecular pathways altered in individual tissues.

Glo1 deficiency affects genes that show genetic association to human metabolic diseases

Although *Glo1* has been previously identified as a candidate gene for human metabolic disorders [1, 8-10], the underlying mechanisms have not been explored. We took advantage of the publicly available summary statistics from large-scale human GWAS and used the Marker Set Enrichment Analysis (MSEA) from the Mergeomics package [35] to evaluate whether the *Glo1* signature genes in individual tissues exhibited an over-representation of human disease risk variants [22]. As shown **(Figure 6D)**, the strongest and most consistent associations of DEGs across tissues were found for four lipid traits (LDL, HDL, TC, TG). We also identified a significant association of the Glo1 DEGs with birth weight, height and waist/hip ratio (WHR). Additionally, consistent with our data – *Glo1*$^{+/-}$ hyperglycemia and dampened glucose tolerance, the liver-specific signatures are associated with fasting glucose, HbA1c and HOMA-IR in human GWAS. Moreover, we observed consistent association of *Glo1* DEGs in different tissues with CAD and T2D. These results indicate that *Glo1* deficiency perturbs genes that have been associated with various human metabolic phenotypes or diseases.

DISCUSSION

To explore the role of partial loss of *Glo1* in metabolic disorders, we conducted a systems biology study of *Glo1*$^{+/-}$ mice. We carried out extensive metabolic phenotyping in both sexes at various ages and further performed transcriptomic profiling of key metabolic tissues, followed by network and integrative genomics analysis to elucidate the underlying regulatory cascades and human disease

relevance **(Figure 7A)**. We found that *Glo1*$^{+/-}$ mice demonstrated metabolic dysregulation, including increased body weight and fat mass in both sexes post-developmentally. Metabolic dysregulation was also observed in a sex-dependent manner, including increased muscle mass and hypoglycemia in male *Glo1*$^{+/-}$ mice, whereas, increased circulating TG and VLDL and compromised glucose tolerance were seen in female *Glo1*$^{+/-}$ mice. The metabolic phenotypes observed in *Glo1*$^{+/-}$ female mice were paralleled by large-scale tissue-specific expression alterations in metabolic genes and pathways across tissues. Select lipid metabolic pathway alterations were also confirmed by qPCR experiments in both males and females. The tissue-specific molecular signatures were further tied to numerous tissue-specific TFs that regulate adipogenesis, insulin signaling, aortic endothelial functions, and key liver functions, and collectively demonstrated significant association with multiple human metabolic traits. Importantly, after quantifying the most prominent AGEs (CEL and MGH1) in metabolic tissues, we found that the observed systemic effects of *Glo1* deficiency cannot be explained by the previously suspected AGE pathway. These findings support a role for *Glo1* in modulating metabolic risks, particularly in adult female mice, through AGE-independent perturbation of metabolic and vascular pathways.

Our observation that *Glo1* deficiency led to increased weight and adiposity is consistent with the previous linkage study that revealed *Glo1* resided under a QTL for body weight in mice [56] and the Wortmann et al. study using the same mouse model in males where increases in weight were not apparent at 10 weeks of age [57]. In females, the body weight increase in *Glo1*$^{+/-}$ mice was largely due to growth of various adipose depots since lean mass remained on par with control

mice, whereas, increased body weight in male *Glo1*$^{+/-}$ mice was attributed to both fat and muscle mass. Along with obesity, the female *Glo1*$^{+/-}$ mice also demonstrated comorbidities such as impaired lipid and glucose homeostasis, phenotypically manifested as hyperlipidemia and glucose intolerance. Surprisingly, male *Glo1*$^{+/-}$ mice showed unaltered glycemic homeostasis but a dysregulated lipid profile with significantly decreased TG, TC, and HDL compared to control mice. In addition, the majority of the perturbed metabolic profiles was observed after 12 weeks of age, suggesting an age-dependent effect in *Glo1*$^{+/-}$ mice. This observation is consistent with the lack of increased body weight previously reported for the *Glo1* deficiency by the Wortmann et al. study using the same mouse model where the follow-up period was only 10 weeks [57]. This implicates the potential of partial *Glo1* deficiency in programming the body towards a state prone to metabolic dysfunctions, which heightens the risk of age-associated metabolic diseases.

Investigation of the female adipose transcriptome revealed changes in a large number of pathways and key regulatory genes involved in adipocyte differentiation, adipocytokine signaling, insulin signaling, and fatty acid/triglyceride biosynthesis. Moreover, we found perturbations in GPCR signaling, PPAR signaling and triglyceride biosynthesis, a state that promotes adipogenesis and subsequent obesity risk [58, 59]. This is further supported by the identification of adipogenic master regulators including PPARG and ATF3 as TF hotspots for the DEGs altered in *Glo1*$^{+/-}$ female mice. The liver gene signatures were significantly enriched for fatty acid metabolism along with bile acid metabolism and glucose metabolism, consistent with the altered TG, VLDL levels and insulin sensitivity in *Glo1*$^{+/-}$ female mice. As males exhibited decreased lipid profiles without glycemic alterations, we further tested genes

involved in lipid metabolism in both sexes using qPCR and found disparate tissue-specific changes in numerous genes (*Fasn*, *Scd1*, *Srebp1c*, etc.) between sexes, providing molecular support for the distinct phenotypic manifestations between males and females. However, we did observe consistent changes in genes such as *Acc1* (fatty acid synthesis) and *Lipin1* (triglyceride synthesis). The different lipid profiles between sexes likely reflect the collective differential activities of the lipid metabolism pathways across tissues between males and females **(Figure 4)**.

Our characterization of sex-specific responses in metabolic traits yielded novel results suggesting that female mice are more vulnerable to *Glo1* deficiency, especially in maintaining glucose homeostasis. We also revealed that 4 out of 17 genes (*Ebp*, *Lss*, *Hsd17b7*, *Nsdhl*) in the steroid synthesis pathway have altered expression exclusively in female adipose tissue (Fold change = 6.3, p = 2.6e-4). As a critical pathway that modulates sexual dimorphic adiposity [14], disruption of steroid synthesis may serve as a mediator for the effect of Glo1 deficiency on adiposity in females. However, we only examined the full transcriptome in females and only tested select lipid genes in both sexes in the current study, therefore, further investigations are warranted to assess additional sexually dimorphic pathways between sexes.

Glo1 has been previously implicated as a key regulator for CAD [8]. We did not observe direct evidence for atherosclerotic lesions in 34-week-old *Glo1*$^{+/-}$ mice, likely due to the natural resistance of mice for atherogenesis without extreme genetic and dietary perturbations. However, the transcriptomic profiling of aorta provided supportive links between *Glo1* deficiency and atherosclerosis. Pathway analysis of the aorta DEGs showed significant alterations related to lysosome and

lipid metabolism, processes implicated in atherogenesis [60, 61]. Additionally, TF prediction for the aorta DEGs identified TFs that are related to circadian rhythms and endothelial inflammation, which are also important processes for atherogenesis [53], [62]. Also, one TF identified in our aorta analysis was TCF21, a basic helix-loop-helix transcription factor, that has been functionally linked to CAD [63, 64]. Furthermore, the Glo1 DEG signatures from multiple tissues examined were also strongly associated with lipid profiles (TG, TC, LDL, HDL) and CAD in human GWAS. The negative atherosclerotic phenotype in *Glo1*$^{+/-}$ mice could be due to insufficient reduction of *Glo1* activity, natural resistance to the development of atherosclerotic lesions and no enforced genetic or environmental stress in our study. Previous studies on the role of Glo1 in atherosclerosis have also yielded inconsistent results. Geoffrion et al. showed that *Glo1* transgene or *Glo1*$^{+/-}$ did not affect the progression of atherosclerosis in the *ApoE*$^{-/-}$ mice at 22 weeks of age, even under diabetic conditions [65]. On the other hand, Jo-Watanabe et al. showed that *Glo1* transgenic mice on *Apoe*$^{-/-}$ background under a high-fat diet went through a reduction of glycation and oxidative stress while preventing age-related endothelial dysfunction by the prevention of eNOS inactivation [66]. Future studies that focus on the long-term effects in atherosclerosis susceptible models with significant genetic or environmental challenges could yield more power in elucidating the potential causal role of *Glo1* in atherosclerosis.

Unexpectedly, *Glo1* deficiency did not lead to increases in AGEs in liver and gonadal adipose tissue in either sex and only male *Glo1*$^{+/-}$ mice showed significantly increased MGH1 in the skeletal muscle. The gene that encodes Rage, *Ager*, was also surprisingly decreased. The common compensatory enzymes such as *Akr1a1* and

Aldh1a1 also did not show consistent changes in the various tissues and between sexes. Overall, these results do not support a major role of AGEs. Although our ability to capture significant AGE changes might be limited by the tissues explored, our findings largely agree with those from the Wortmann et al. study which did not detect a difference in AGEs in heart, kidney and liver between *Glo1*$^{+/-}$ and WT [55]. These findings could suggest the glyoxalase system is robust in nature and therefore able to compensate under stressful conditions. Furthermore, the results could also suggest that a defective glyoxalase system has an untapped regulatory circuit for metabolic function that is independent of the well-known "dicarbonyl stress" [10]. For instance, we identified novel candidates that potentially mediate the downstream effect of *Glo1* deficiency such as dysregulation of the circadian clock, adipogenesis, fatty acid metabolism, and PPAR signaling. *Per2* (Period Circadian Regulator 2), a primary circadian pacemaker, was consistently upregulated in adipose (Fold = 2.63, p = 1.8e-2) and aorta (Fold = 2.09, p = 1.9e-3). Moreover, the downstream targets of several TFs involved in circadian clock regulation such as ARNTL were found to have perturbed expression in aorta. The extensive perturbation of numerous metabolic pathways in individual tissues through regulatory genes such as PPARg, ATF3, and HNF4A, which are among the top ten transcription factors predicted to regulate the altered genes in *Glo1* deficiency, implicate that *Glo1* modulates these metabolic regulators to affect metabolic risks.

Importantly, our integrative genomics analyses coupling the *Glo1* signatures with human genetic studies help connect *Glo1* with numerous human metabolic traits/diseases. These results are largely consistent with the phenotypic profiles

observed in mice and substantiate the relevance of *Glo1* to human metabolic diseases. However, we note a discrepancy in cholesterol phenotypes between our mouse model and the human GWAS integration results which agrees with the previously observed dissimilarity in dyslipidemia between mouse models and humans [67].

In summary, our findings support the role of *Glo1* deficiency in modulating obesity and metabolic dysfunction in a sex specific manner without strong evidence for the involvement of AGEs. Our discoveries regarding tissue-specific genes, pathways and transcription factor hotspots involved in metabolic regulation that are downstream of *Glo1* deficiency in multiple metabolic tissues support broader molecular functions of Glo1 beyond its known role in the glyoxalase system. Moreover, the application of these findings to human disease further supports the importance of exploring the physiological functions and pathogenic potential of *Glo1.*

TABLES

Table 1. Top 10 transcription factors whose downstream targets are enriched for Glo1 deficiency DEG signatures in adipose tissue, aorta and liver.

Adipose			Aorta			Liver		
TF	**Fold**	**P value**	**TF**	**Fold**	**P value**	**TF**	**Fold**	**P value**
KLF12	2.26	2.95E-07	TFAP4	2.32	6.92E-06	HNF4A	2.66	2.42E-10
FOXI1	4.05	1.71E-05	BHLHE40	2.60	1.52E-05	CDX	16.16	2.04E-09
PPARA	2.79	6.90E-05	POU3F3	2.70	6.76E-05	HNF1	3.72	2.05E-09
ETS	2.09	9.11E-05	FOXA	2.80	9.79E-05	SRY	8.46	3.27E-09
FOXD3	4.51	1.48E-04	MAX	4.50	1.43E-04	FOXJ3	4.04	1.19E-08
SPIC	2.74	2.05E-04	BHLHE41	2.59	1.69E-04	PBX1	5.59	2.36E-08
ATF3	2.23	2.16E-04	TFEB	2.22	1.76E-04	ZNF35	9.09	2.60E-08
PPARG	2.18	5.39E-04	POU2F3	2.33	2.21E-04	NKX2-8	11.91	4.49E-08
ETV7	1.95	5.52E-04	TCF21	3.09	2.35E-04	FOXJ2	3.52	1.48E-07
GATA5	4.00	7.09E-04	ARNTL	2.20	3.45E-04	NKX2-2	12.12	2.35E-07

* Exclusion criteria: 1. TF with > 1 000 downstream targets; 2. Number of overlapping genes between TF targets and Glo1 deficiency signatures < 5; 3. Fold enrichment < 2; 4. Overlap ratio between two TFs > 10%. Significance p values were determined using Fisher's exact test.

FIGURES

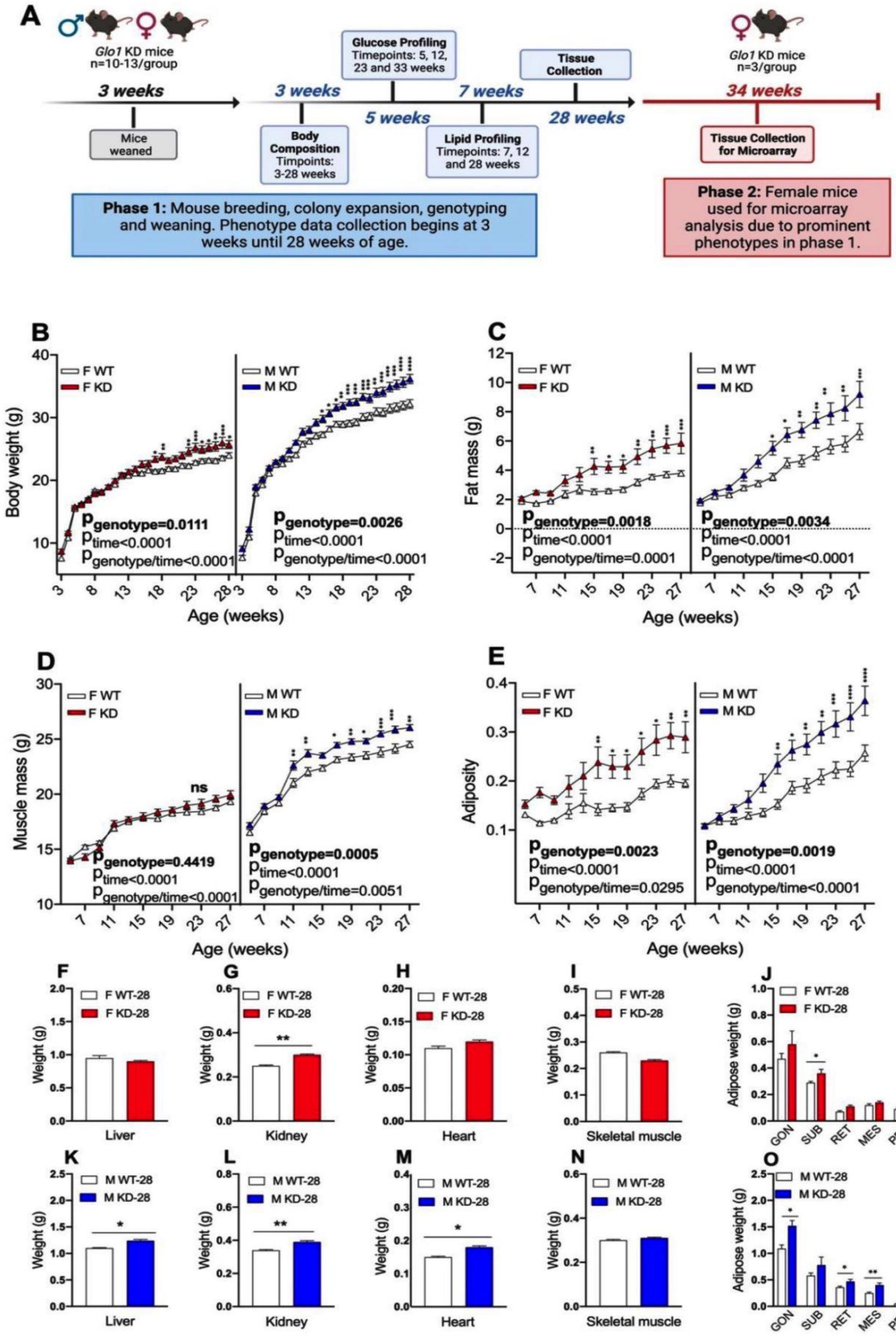
A
Glo1 KD mice
n=10-13/group
3 weeks
Mice weaned
3 weeks
Body Composition
Timpoints:
3-28 weeks
Glucose Profiling
Timepoints: 5, 12, 23 and 33 weeks
5 weeks
7 weeks
Lipid Profiling
Timepoints: 7, 12 and 28 weeks
Tissue Collection
28 weeks
Glo1 KD mice
n=3/group
34 weeks
Tissue Collection for Microarray
Phase 1: Mouse breeding, colony expansion, genotyping and weaning. Phenotype data collection begins at 3 weeks until 28 weeks of age.
Phase 2: Female mice used for microarray analysis due to prominent phenotypes in phase 1.
B
Body weight (g)
F WT
F KD
M WT
M KD
pgenotype=0.0111
ptime<0.0001
pgenotype/time<0.0001
pgenotype=0.0026
ptime<0.0001
pgenotype/time<0.0001
Age (weeks)
C
Fat mass (g)
pgenotype=0.0018
ptime<0.0001
pgenotype/time=0.0001
pgenotype=0.0034
ptime<0.0001
pgenotype/time<0.0001
Age (weeks)
D
Muscle mass (g)
ns
pgenotype=0.4419
ptime<0.0001
pgenotype/time<0.0001
pgenotype=0.0005
ptime<0.0001
pgenotype/time=0.0051
Age (weeks)
E
Adiposity
pgenotype=0.0023
ptime<0.0001
pgenotype/time=0.0295
pgenotype=0.0019
ptime<0.0001
pgenotype/time<0.0001
Age (weeks)
F
G
H
I
J
F WT-28
F KD-28
Weight (g)
Liver
Kidney
Heart
Skeletal muscle
Adipose weight (g)
GON
SUB
RET
MES
PER
K
L
M
N
O
M WT-28
M KD-28

Figure 1. Characterization of body composition phenotypes in *Glo1* deficient mice

(A) Overview of experimental design showing two phases. Phase 1 includes mouse colony expansion and phenotype data collection of mice from weaning at 3 weeks of age until 28 weeks of age. In phase 2, tissues of female mice at age 34 weeks (n=3/group) are collected for microarray analysis due to prominent phenotypes observed in phase 1. **(B)** Body weight for female (n=12-13/group) and male (n=11-14/group) mice were monitored weekly starting from weaning (3 weeks) until 28 weeks of age. **(C)** Fat mass and **(D)** muscle mass was monitored biweekly starting from age 5 weeks of age until 27 weeks of age. **(E)** Adiposity (fat to muscle mass ratio) was monitored biweekly starting from age 5 weeks until 27 weeks. Female **(F)** liver, **(G)** kidney, **(H)** heart and **(I)** bilateral skeletal muscle tissue was weighed at 28 weeks of age. **(J)** Female adipose tissues including gonadal, subcutaneous, retroperitoneal, mesenteric and perirenal adipose tissues were weighed at 28 weeks of age. Male **(K)** liver, **(L)** kidney, (**M)** heart and **(N)** bilateral skeletal muscle tissue was weighed at 28 weeks of age. **(O)** Male adipose tissues including gonadal, subcutaneous, retroperitoneal, mesenteric and perirenal adipose tissue were weighed at 28 weeks of age. Data is shown as mean ± SEM and analyzed using 2-way ANOVA with repeated measures to obtain the statistical significance of the main effects of genotype and time as well the interaction between genotype and time. For individual time points, the difference between genotypes is assessed using the post-hoc Bonferroni's multiple comparisons corrections following 2-way ANOVA with repeated measures. *$p<0.05$, **$p<0.01$, ***$p<0.001$.

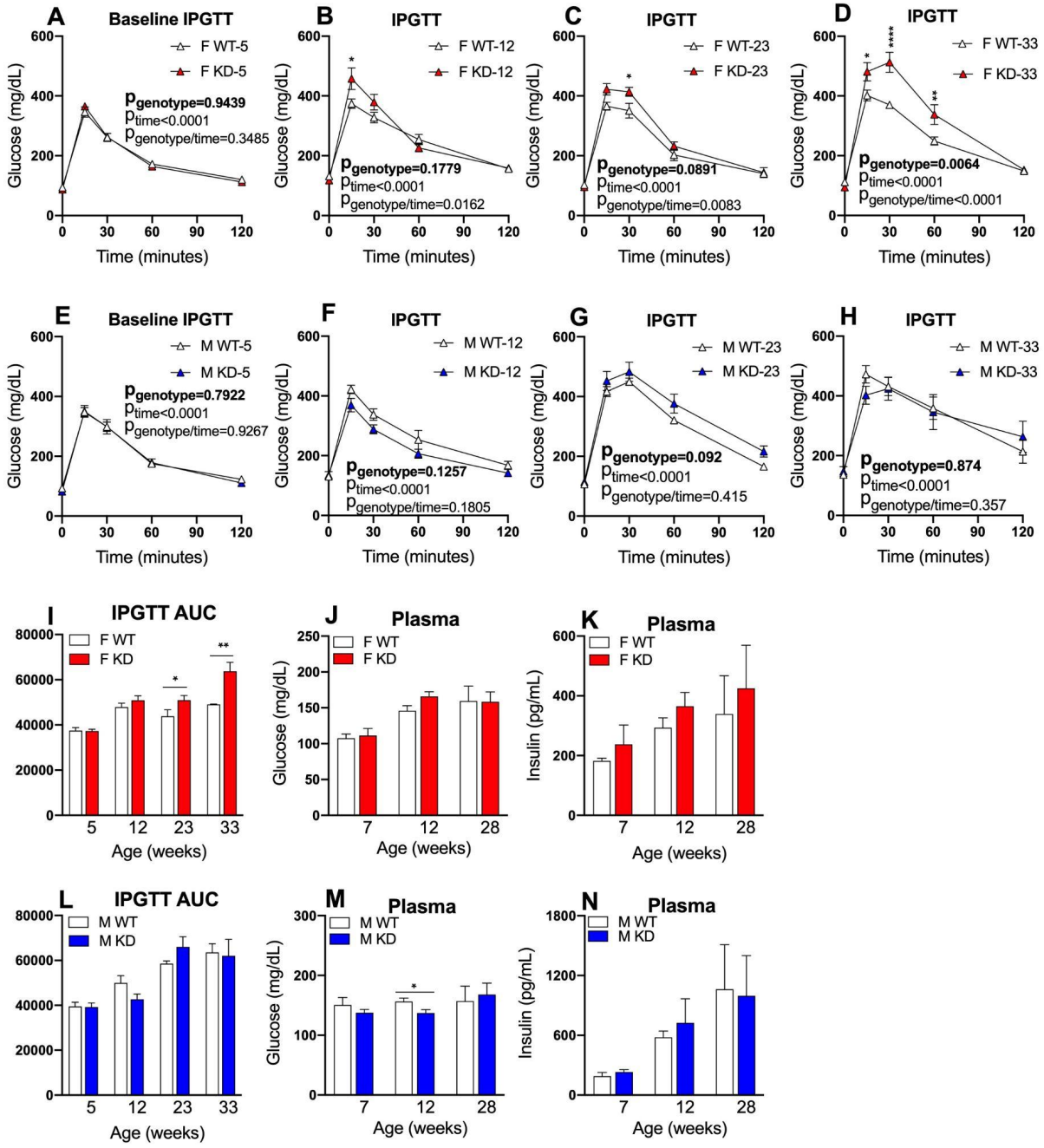
A
Baseline IPGTT
F WT-5
F KD-5
$p_{genotype=0.9439}$
$p_{time<0.0001}$
$p_{genotype/time=0.3485}$
B
IPGTT
F WT-12
F KD-12
$p_{genotype=0.1779}$
$p_{time<0.0001}$
$p_{genotype/time=0.0162}$
C
IPGTT
F WT-23
F KD-23
$p_{genotype=0.0891}$
$p_{time<0.0001}$
$p_{genotype/time=0.0083}$
D
IPGTT
F WT-33
F KD-33
$p_{genotype=0.0064}$
$p_{time<0.0001}$
$p_{genotype/time<0.0001}$
E
Baseline IPGTT
M WT-5
M KD-5
$p_{genotype=0.7922}$
$p_{time<0.0001}$
$p_{genotype/time=0.9267}$
F
IPGTT
M WT-12
M KD-12
$p_{genotype=0.1257}$
$p_{time<0.0001}$
$p_{genotype/time=0.1805}$
G
IPGTT
M WT-23
M KD-23
$p_{genotype=0.092}$
$p_{time<0.0001}$
$p_{genotype/time=0.415}$
H
IPGTT
M WT-33
M KD-33
$p_{genotype=0.874}$
$p_{time<0.0001}$
$p_{genotype/time=0.357}$
Glucose (mg/dL)
Time (minutes)
I
IPGTT AUC
F WT
F KD
Age (weeks)
J
Plasma
K
Plasma
Insulin (pg/mL)
L
IPGTT AUC
M WT
M KD
M
Plasma
N
Plasma

Figure 2. Characterization of glucose metabolism phenotypes in *Glo1* deficient mice

(A) Baseline intraperitoneal glucose tolerance test (IPGTT) was performed on fasted female mice at 5 weeks of age (n=13). Follow up IPGTT experiments were performed on female mice at **(B)** 12 (n=13), **(C)** 23 (n=13) and **(D)** 33 weeks of age (n=5). **(I)** Quantification for area under the curve (AUC) was determined for female mice for all time points. **(E)** Baseline IPGTT was performed on fasted male mice at 5 weeks of age (n=13). Follow up IPGTT experiments were performed on male mice at **(F)** 12 (n=13), **(G)** 23 (n=13) and **(H)** 33 weeks of age (n=5). **(L)** Quantification for area under the curve (AUC) was determined for male mice for all time points. Blood plasma **(J)** glucose and **(K)** insulin levels were quantified in fasted female mice at 7 (n=9), 12 (n=9) and 28 weeks of age (n=9). Blood plasma **(M)** glucose and **(N)** insulin levels were quantified in fasted male mice at 7 (n=9), 12 (n=9) and 28 weeks of age (n=9). IPGTT data was analyzed using 2-way ANOVA followed by Bonferroni's multiple comparisons tests to obtain the statistical significance of the main effects of genotype and time as well the interaction between genotype and time. AUC data was analyzed using 1-way ANOVA followed by Bonferroni's multiple comparisons tests. *p<0.05, **p<0.01, ***p<0.001. Plasma glucose and insulin data is presented as mean ± SEM and statistical significance among groups was calculated by Student t-test. *p<0.05, **p<0.01, ***p<0.001.

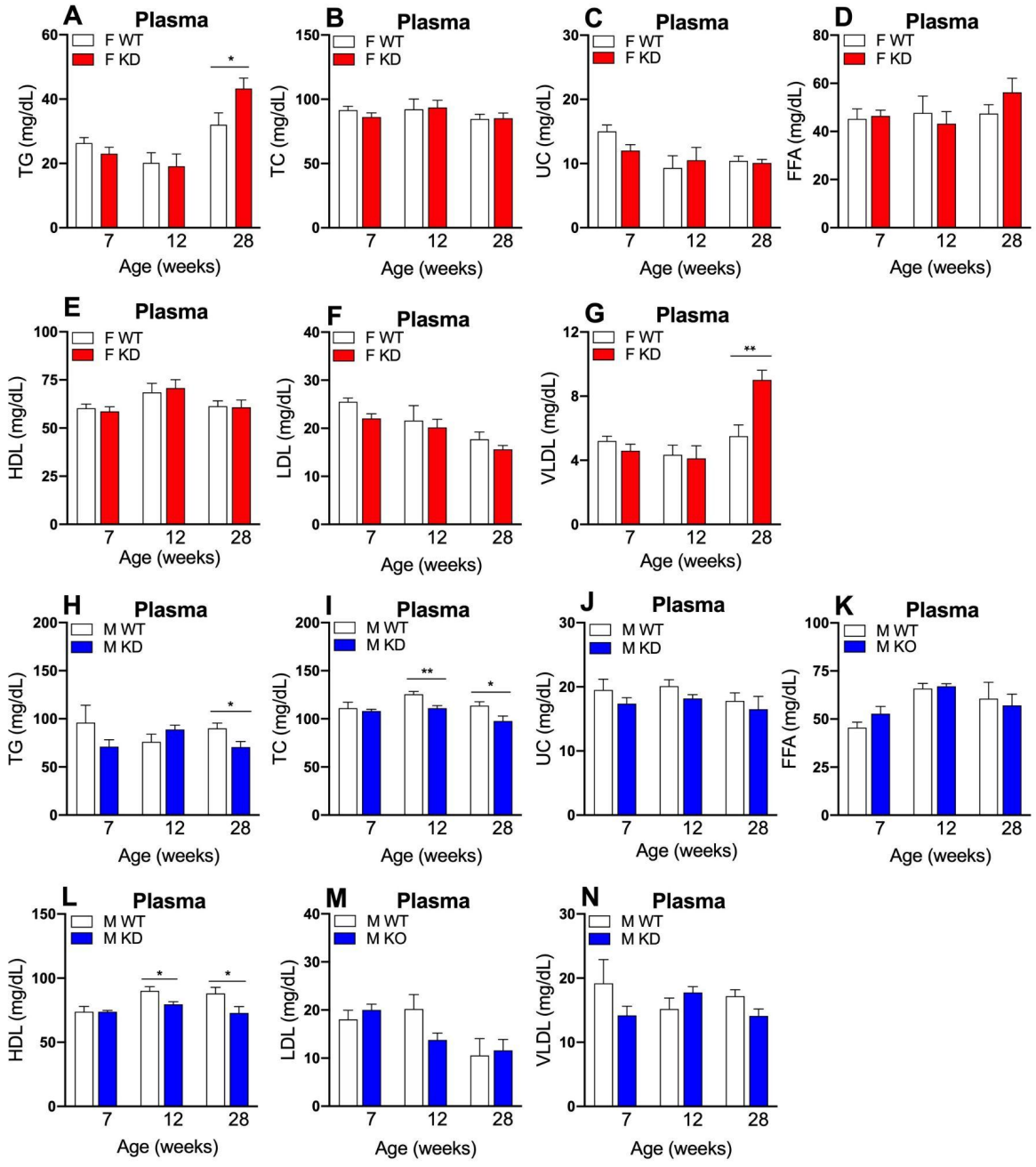
A
Plasma
F WT
F KD
TG (mg/dL)
Age (weeks)
B
Plasma
TC (mg/dL)
C
Plasma
UC (mg/dL)
D
Plasma
FFA (mg/dL)
E
Plasma
HDL (mg/dL)
F
Plasma
LDL (mg/dL)
G
Plasma
VLDL (mg/dL)
H
Plasma
M WT
M KD
I
Plasma
J
Plasma
K
Plasma
M KO
L
Plasma
M
Plasma
N
Plasma

Figure 3. Lipid profiling quantification in *Glo1* deficient mice

Plasma lipoproteins **(A)** triglycerides (TG), **(B)** total cholesterol (TC), **(C)** unesterified cholesterol (UC), **(D)** free fatty acids (FFA), **(E)** high-density lipoprotein (HDL), **(F)** low-density lipoprotein (LDL) and **(G)** very low-density lipoprotein (VLDL) were quantified in 14-hour fasted female mice at 7 (n=9), 12 (n=9) and 28 (n=9) weeks of age**.** Plasma lipoproteins **(H)** TG, **(I)** TC, **(J)** UC, **(K)** FFA, **(L)** HDL, **(M)** LDL and **(N)** VLDL were quantified in 14-hour fasted male mice at 7 (n=9), 12 (n=9) and 28 (n=9) weeks of age. Data is presented as mean ± SEM and statistical significance among groups was calculated by Student t-test. *p<0.05, **p<0.01, ***p<0.001.

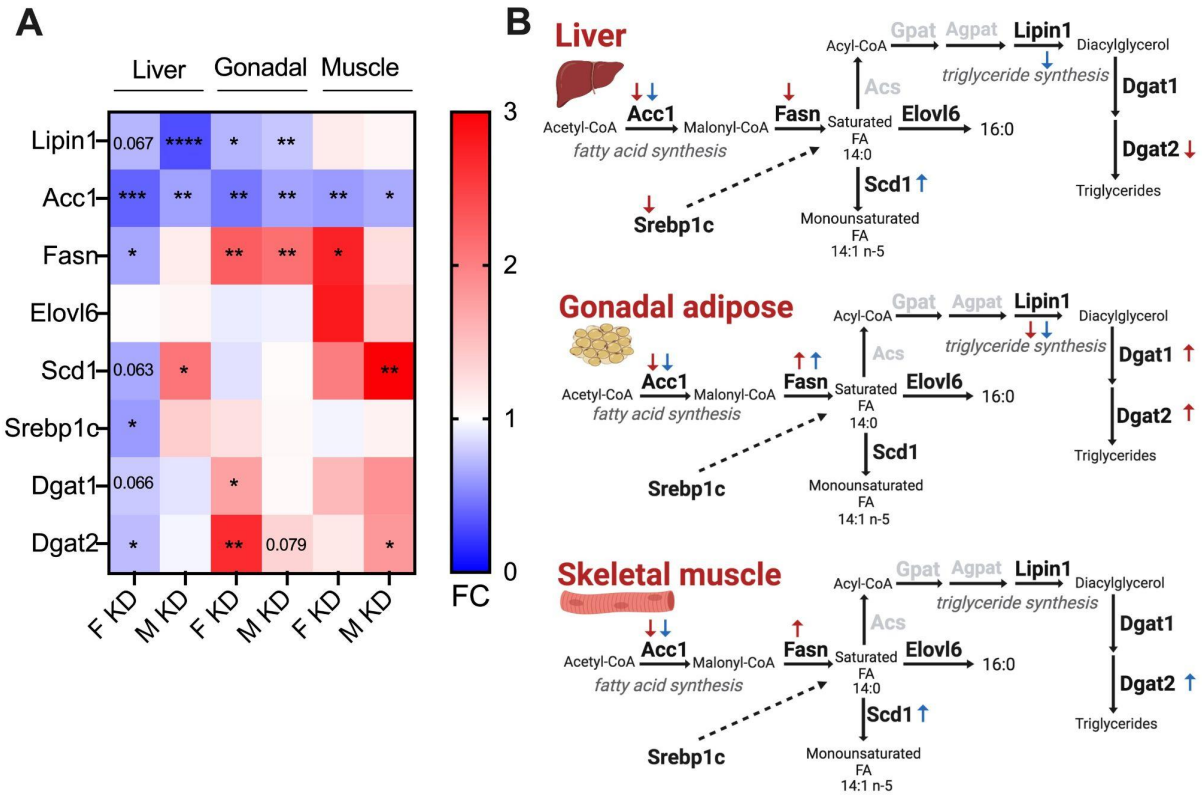
A
Liver
Gonadal
Muscle
Lipin1
Acc1
Fasn
Elovl6
Scd1
Srebp1c
Dgat1
Dgat2
0.067
****
*
**
***
**
**
**
**
*
*
**
**
*
*
0.063
*
**
*
0.066
*
*
**
0.079
*
F KD
M KD
F KD
M KD
F KD
M KD
3
2
1
0
FC
B
Liver
Acyl-CoA
Gpat
Agpat
Lipin1
Diacylglycerol
triglyceride synthesis
Dgat1
Dgat2
Triglycerides
Acs
Acetyl-CoA
Acc1
Malonyl-CoA
Fasn
Saturated FA 14:0
Elovl6
16:0
fatty acid synthesis
Srebp1c
Scd1
Monounsaturated FA 14:1 n-5
Gonadal adipose
Skeletal muscle

Figure 4. Expression of lipid metabolism genes across liver, gonadal adipose and skeletal muscle tissues in *Glo1* deficient mice

(A) Using qPCR, expression of lipid metabolism genes (*Lipin1, Acc1, Fasn Elovl6, Scd1, Srebp1c, Dgat1, Dgat2*) were assessed in liver, gonadal adipose and skeletal muscle tissue and in 28-week-old female and male mice (n=4/group). **(B)** Lipid metabolism pathway in liver, gonadal adipose and skeletal muscle tissue is shown to reflect significant changes in gene expression with red arrows depicting female *Glo1* deficient mice and blue arrows for male *Glo1* deficient mice. Arrows pointing up depict significantly upregulated mRNA expression and arrows pointing down depict significantly downregulated mRNA expression. Genes that encode enzymes involved in lipid metabolism pathway but not tested are represented by the gray color (*Acs, Gpat, Agpat*). Data was analyzed using unpaired t-test with Welch's correction. Statistically significant data is denoted by *p<0.05, **p<0.01, ***p<0.001, ****p>0.0001.

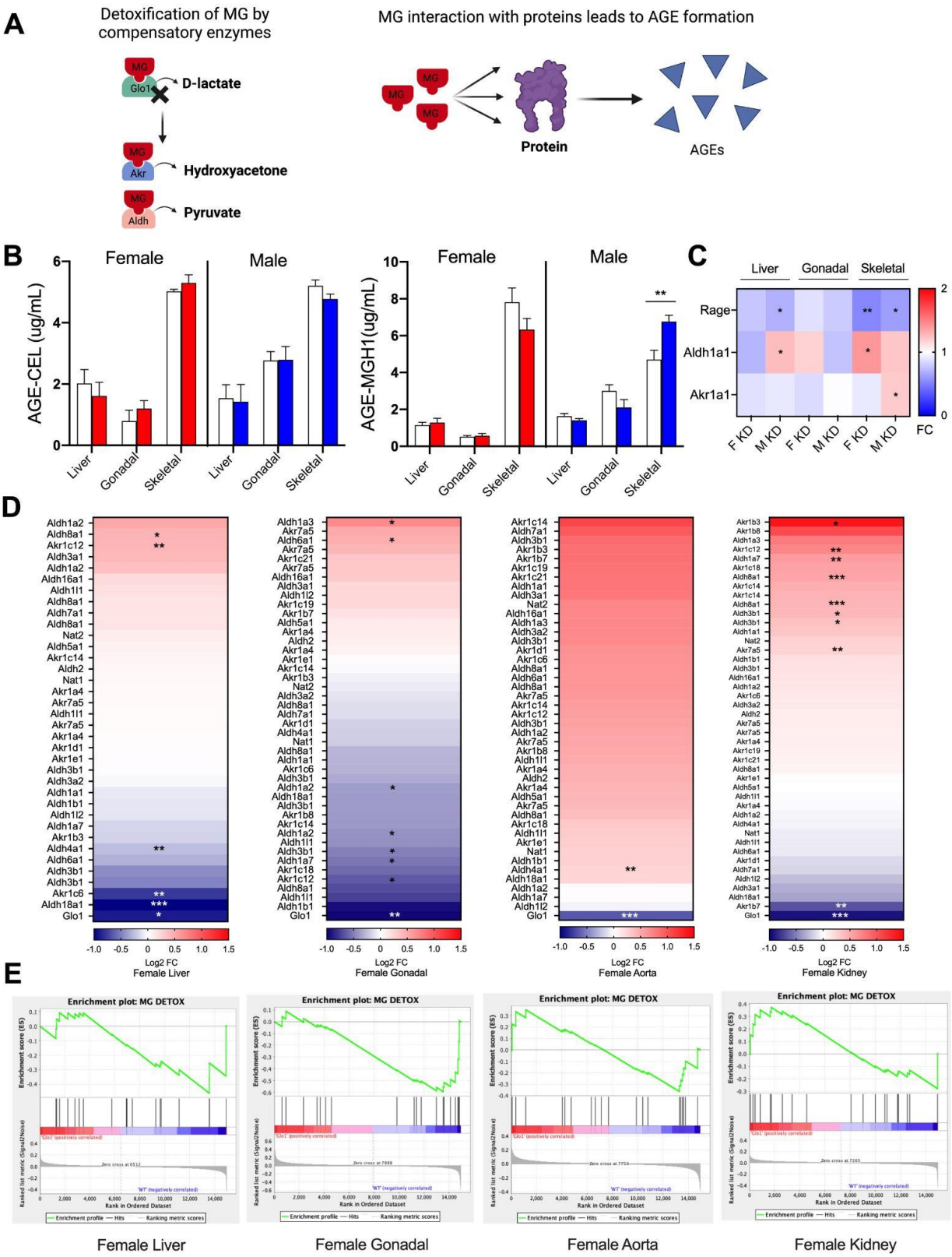
A
Detoxification of MG by compensatory enzymes
MG
Glo1
D-lactate
MG
Akr
Hydroxyacetone
MG
Aldh
Pyruvate
MG interaction with proteins leads to AGE formation
MG
MG
MG
Protein
AGEs
B
Female
Male
AGE-CEL (ug/mL)
AGE-MGH1(ug/mL)
Liver
Gonadal
Skeletal
C
Liver
Gonadal
Skeletal
Rage
Aldh1a1
Akr1a1
F KD
M KD
FC
D
Log2 FC
Female Liver
Female Gonadal
Female Aorta
Female Kidney
E
Enrichment plot: MG DETOX
Enrichment score (ES)
Ranked list metric (Signal2Noise)
Rank in Ordered Dataset
Enrichment profile
Hits
Ranking metric scores
Female Liver
Female Gonadal
Female Aorta
Female Kidney

Figure 5. Assessment of AGEs and AGE-related components across liver, gonadal adipose and skeletal muscle tissues in *Glo1* deficient mice

(A) Overview mechanism of alternate MG detoxification by compensatory enzymes Akr and Aldh (left). Overview mechanism of MG interaction with proteins leading to the generation of AGEs (right). **(B)** Quantification by ELISA of CEL (left) and MGH1 (right) in female and male mice at 28 weeks of age across metabolic tissues including liver, gonadal adipose and skeletal muscle (n=6-7/group). **(C)** mRNA expression for Rage, Akr1a1 and Aldh1a1 across liver, gonadal adipose and skeletal muscle tissues (n=5-6/group). **(D)** Microarray analysis shows changes in gene expression for compensatory enzymes (Akr and Aldh subtypes) across metabolic tissues including liver, gonadal adipose, aorta and kidney in *Glo1* deficient female mice at 34 weeks of age. **(E)** Gene set enrichment analysis (GSEA) plots from curated DEG list for compensatory enzymes (Akr and Aldh subtypes) across metabolic tissues including liver, gonadal adipose, aorta and kidney in *Glo1* deficient female mice at 34 weeks of age. Enrichment score (ES) was calculated to determine significance of GSEA plot. ELISA and qPCR data was analyzed using unpaired t-test with Welch's correction. Microarray data was analyzed using unpaired t-test. Statistically significant data is denoted by *p<0.05, **p<0.01, ***p<0.001, ****p>0.0001.

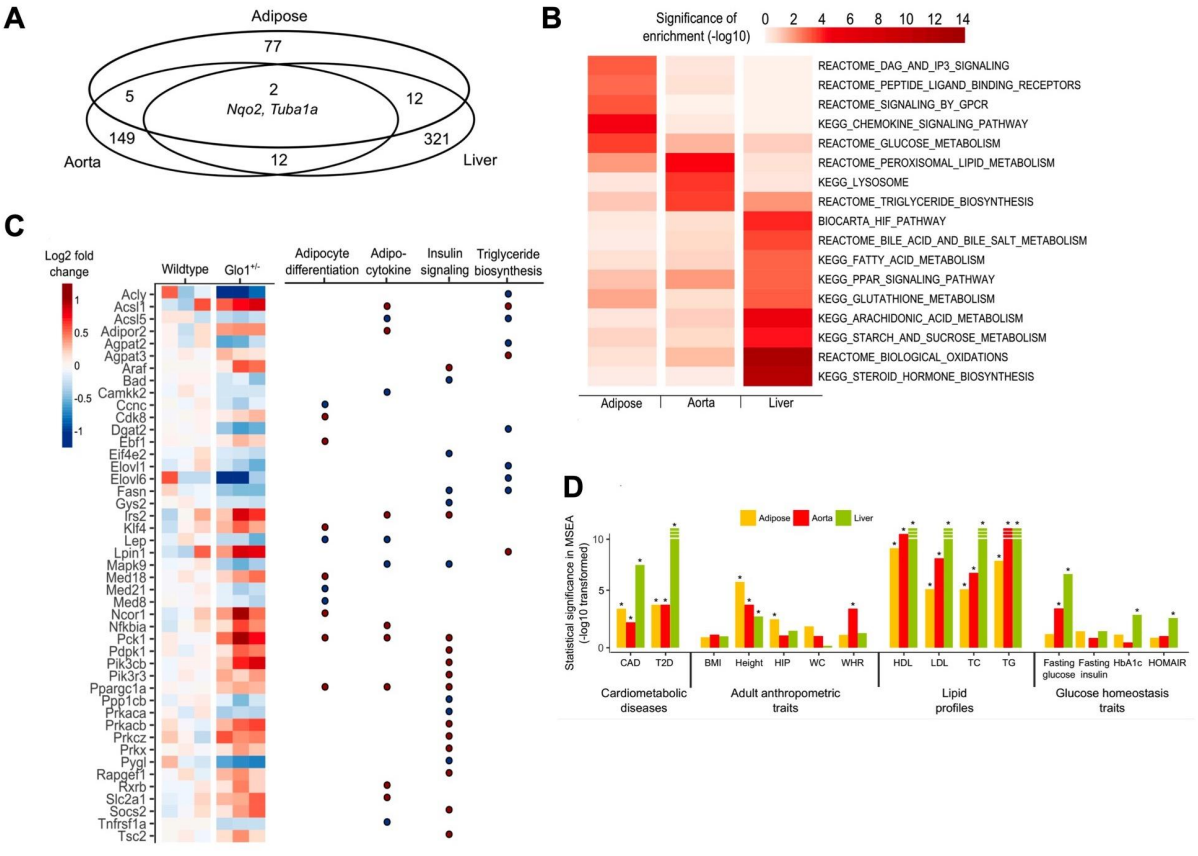
A
Adipose
77
5
2
Nqo2, Tuba1a
12
149
321
Aorta
12
Liver
B
Significance of enrichment (-log10)
0 2 4 6 8 10 12 14
REACTOME_DAG_AND_IP3_SIGNALING
REACTOME_PEPTIDE_LIGAND_BINDING_RECEPTORS
REACTOME_SIGNALING_BY_GPCR
KEGG_CHEMOKINE_SIGNALING_PATHWAY
REACTOME_GLUCOSE_METABOLISM
REACTOME_PEROXISOMAL_LIPID_METABOLISM
KEGG_LYSOSOME
REACTOME_TRIGLYCERIDE_BIOSYNTHESIS
BIOCARTA_HIF_PATHWAY
REACTOME_BILE_ACID_AND_BILE_SALT_METABOLISM
KEGG_FATTY_ACID_METABOLISM
KEGG_PPAR_SIGNALING_PATHWAY
KEGG_GLUTATHIONE_METABOLISM
KEGG_ARACHIDONIC_ACID_METABOLISM
KEGG_STARCH_AND_SUCROSE_METABOLISM
REACTOME_BIOLOGICAL_OXIDATIONS
KEGG_STEROID_HORMONE_BIOSYNTHESIS
Adipose
Aorta
Liver
C
Log2 fold change
1
0.5
0
-0.5
-1
Wildtype
Glo1+/-
Adipocyte differentiation
Adipo-cytokine
Insulin signaling
Triglyceride biosynthesis
Acly
Acsl1
Acsl5
Adipor2
Agpat2
Agpat3
Araf
Bad
Camkk2
Ccnc
Cdk8
Dgat2
Ebf1
Eif4e2
Elovl1
Elovl6
Fasn
Gys2
Irs2
Klf4
Lep
Lpin1
Mapk9
Med18
Med21
Med8
Ncor1
Nfkbia
Pck1
Pdpk1
Pik3cb
Pik3r3
Ppargc1a
Ppp1cb
Prkaca
Prkacb
Prkcz
Prkx
Pygl
Rapgef1
Rxrb
Slc2a1
Socs2
Tnfrsf1a
Tsc2
D
Statistical significance in MSEA (-log10 transformed)
Adipose
Aorta
Liver
10
5
0
CAD
T2D
BMI
Height
HIP
WC
WHR
HDL
LDL
TC
TG
Fasting glucose
Fasting insulin
HbA1c
HOMAIR
Cardiometabolic diseases
Adult anthropometric traits
Lipid profiles
Glucose homeostasis traits

Figure 6. Summary of differentially expressed gene signatures in *Glo1* deficient mice and genetic association to human metabolic diseases

(A) Venn diagram of the number of significant DEGs with FDR < 10% in adipose, aorta and liver. **(B)** Individual sample expression level changes for genes involved in adipocyte differentiation, adipocytokine and insulin signaling with significant expression level difference with P < 0.05. Fold change was determined by comparing the expression values of $Glo1^{+/-}$ mice to the mean value of wildtype samples. Red and blue indicate increased and decreased expression in knockdown mice, respectively. **(C)** Canonical pathways with enrichment FDR < 5% are shown. Statistical significance was determined by Fisher's exact test. **(D)** For human metabolic trait association, statistical significance was determined by MSEA. Asterisks indicate a significant association with FDR<5%. Results with p-values (–log10 transformed) larger than 10 are capped at 10. CAD, coronary artery disease; T2D, type 2 diabetes; BMI, body mass index; HIP, hip circumference; WC, waist circumference; WHR, waist-hip ratio.

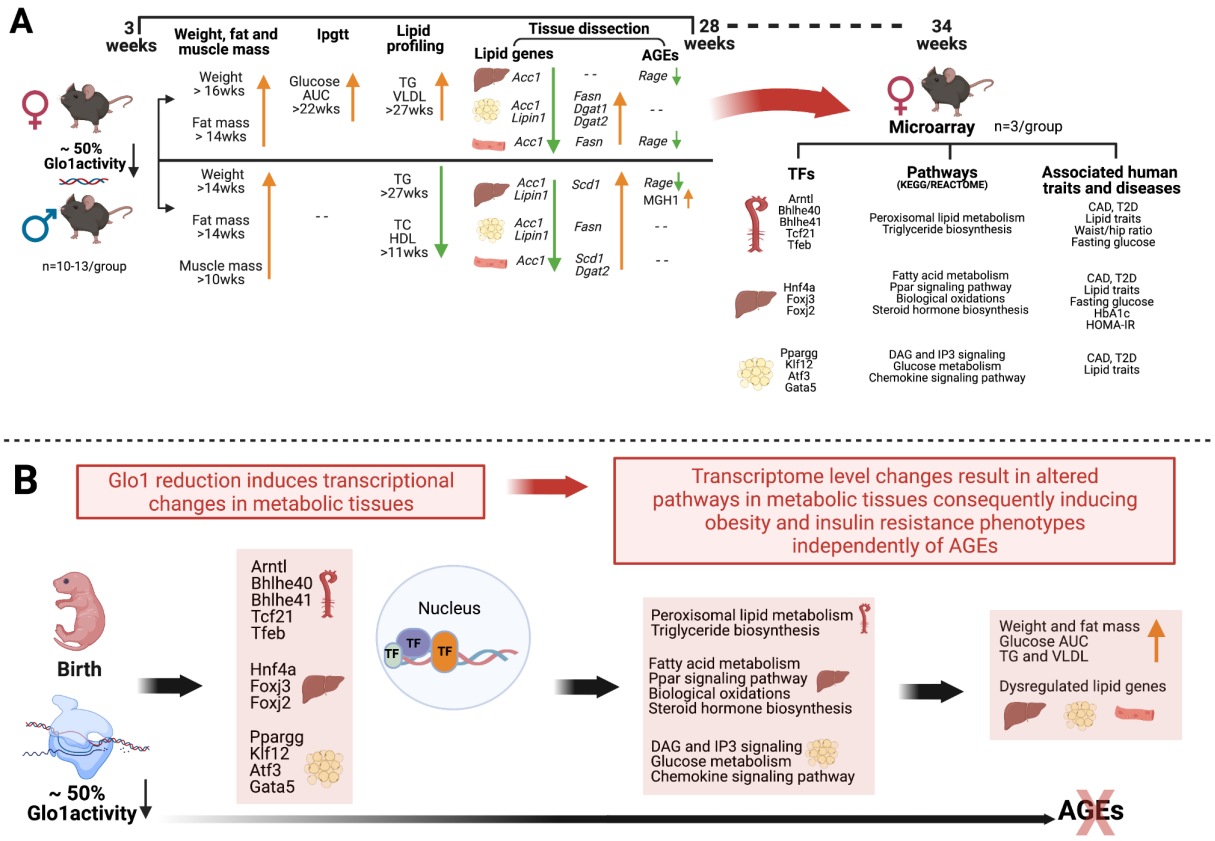
A
3 weeks
Weight, fat and muscle mass
Ipgtt
Lipid profiling
Tissue dissection
Lipid genes
AGEs
28 weeks
34 weeks
~ 50% Glo1activity
n=10-13/group
Weight > 16wks
Fat mass > 14wks
Glucose AUC >22wks
TG VLDL >27wks
Acc1
Acc1 Lipin1
Acc1
Fasn
Fasn Dgat1 Dgat2
Fasn
Rage
Rage
Weight >14wks
Fat mass >14wks
Muscle mass >10wks
TG >27wks
TC HDL >11wks
Acc1 Lipin1
Acc1 Lipin1
Acc1
Scd1
Fasn
Scd1 Dgat2
Rage
MGH1
Microarray
n=3/group
TFs
Pathways (KEGG/REACTOME)
Associated human traits and diseases
Arntl Bhlhe40 Bhlhe41 Tcf21 Tfeb
Peroxisomal lipid metabolism
Triglyceride biosynthesis
CAD, T2D
Lipid traits
Waist/hip ratio
Fasting glucose
Hnf4a Foxj3 Foxj2
Fatty acid metabolism
Ppar signaling pathway
Biological oxidations
Steroid hormone biosynthesis
CAD, T2D
Lipid traits
Fasting glucose
HbA1c
HOMA-IR
Ppargg Klf12 Atf3 Gata5
DAG and IP3 signaling
Glucose metabolism
Chemokine signaling pathway
CAD, T2D
Lipid traits

B
Glo1 reduction induces transcriptional changes in metabolic tissues
Transcriptome level changes result in altered pathways in metabolic tissues consequently inducing obesity and insulin resistance phenotypes independently of AGEs
Birth
~ 50% Glo1activity
Arntl Bhlhe40 Bhlhe41 Tcf21 Tfeb
Hnf4a Foxj3 Foxj2
Ppargg Klf12 Atf3 Gata5
Nucleus
TF
TF
TF
Peroxisomal lipid metabolism
Triglyceride biosynthesis
Fatty acid metabolism
Ppar signaling pathway
Biological oxidations
Steroid hormone biosynthesis
DAG and IP3 signaling
Glucose metabolism
Chemokine signaling pathway
Weight and fat mass
Glucose AUC
TG and VLDL
Dysregulated lipid genes
AGEs

Figure 7. Schematic summary of *Glo1* deficit effects in female and male mice

(A) Schematic overview of study design showing the metabolic phenotypes induced by *Glo 1* deficiency in female and male mice overtime. **(B)** Proposed mechanism of *Glo1* deficiency effects on transcriptome inducing metabolic dysfunction in female mice.

BIBLIOGRAPHY

1. Masania, J., et al., *Dicarbonyl stress in clinical obesity.* Glycoconj J, 2016. 33(4): p. 581-9.

2. Rabbani, N. and P.J. Thornalley, *Glyoxalase 1 Modulation in Obesity and Diabetes.* Antioxid Redox Signal, 2019. 30(3): p. 354-374.

3. Xue, M., et al., *Improved Glycemic Control and Vascular Function in Overweight and Obese Subjects by Glyoxalase 1 Inducer Formulation.* Diabetes, 2016. 65(8): p. 2282-94.

4. Song, F. and A.M. Schmidt, *Glycation and insulin resistance: novel mechanisms and unique targets?* Arterioscler Thromb Vasc Biol, 2012. 32(8): p. 1760-5.

5. Stratmann, B., et al., *Glyoxalase 1-knockdown in human aortic endothelial cells - effect on the proteome and endothelial function estimates.* Sci Rep, 2016. 6: p. 37737.

6. Spanos, C., et al., *Proteomic identification and characterization of hepatic glyoxalase 1 dysregulation in non-alcoholic fatty liver disease.* Proteome Sci, 2018. 16: p. 4.

7. Mey, J.T. and J.M. Haus, *Dicarbonyl Stress and Glyoxalase-1 in Skeletal Muscle: Implications for Insulin Resistance and Type 2 Diabetes.* Front Cardiovasc Med, 2018. 5: p. 117.

8. Makinen, V.P., et al., *Integrative genomics reveals novel molecular pathways and gene networks for coronary artery disease.* PLoS Genet, 2014. 10(7): p. e1004502.

9. Maessen, D.E., C.D. Stehouwer, and C.G. Schalkwijk, *The role of methylglyoxal and the glyoxalase system in diabetes and other age-related diseases.* Clin Sci (Lond), 2015. 128(12): p. 839-61.

10. Rabbani, N., M. Xue, and P.J. Thornalley, *Methylglyoxal-induced dicarbonyl stress in aging and disease: first steps towards glyoxalase 1-based treatments.* Clin Sci (Lond), 2016. 130(19): p. 1677-96.

11. Rabbani, N. and P.J. Thornalley, *Glyoxalase in diabetes, obesity and related disorders.* Semin Cell Dev Biol, 2011. 22(3): p. 309-17.

12. Booth, I.R., *Glycerol and Methylglyoxal Metabolism.* EcoSal Plus, 2005. 1(2).

13. Schumacher, D., et al., *Compensatory mechanisms for methylglyoxal detoxification in experimental & clinical diabetes.* Mol Metab, 2018. 18: p. 143-152.

14. Thornalley, P.J., *Glycation in diabetic neuropathy: characteristics, consequences, causes, and therapeutic options.* Int Rev Neurobiol, 2002. 50: p. 37-57.

15. Palma-Duran, S.A., et al., *Serum levels of advanced glycation end-products (AGEs) and the decoy soluble receptor for AGEs (sRAGE) can identify non-alcoholic fatty liver disease in age-, sex- and BMI-matched normo-glycemic adults.* Metabolism, 2018. 83: p. 120-127.

16. Hori, O., et al., *The receptor for advanced glycation end-products has a central role in mediating the effects of advanced glycation end-products on the development of vascular disease in diabetes mellitus.* Nephrol Dial Transplant, 1996. 11 Suppl 5: p. 13-6.

17. Choi, B.R., et al., *Increased expression of the receptor for advanced glycation end products in neurons and astrocytes in a triple transgenic mouse model of Alzheimer's disease.* Exp Mol Med, 2014. 46: p. e75.

18. Queisser, M.A., et al., *Hyperglycemia impairs proteasome function by methylglyoxal.* Diabetes, 2010. 59(3): p. 670-8.

19. Xue, M., N. Rabbani, and P.J. Thornalley, *Glyoxalase in ageing.* Semin Cell Dev Biol, 2011. 22(3): p. 293-301.

20. Hedrick, C.C., et al., *Influence of mouse apolipoprotein A-II on plasma lipoproteins in transgenic mice.* J Biol Chem, 1993. 268(27): p. 20676-82.

21. Du, P., W.A. Kibbe, and S.M. Lin, *lumi: a pipeline for processing Illumina microarray.* Bioinformatics, 2008. 24(13): p. 1547-8.

22. Storey, J.D. and R. Tibshirani, *Statistical significance for genomewide studies.* Proc Natl Acad Sci U S A, 2003. 100(16): p. 9440-5.

23. Kanehisa, M. and S. Goto, *KEGG: kyoto encyclopedia of genes and genomes.* Nucleic Acids Res, 2000. 28(1): p. 27-30.

24. Matthews, L., et al., *Reactome knowledgebase of human biological pathways and processes.* Nucleic Acids Res, 2009. 37(Database issue): p. D619-22.

25. Ashburner, M., et al., *Gene ontology: tool for the unification of biology. The Gene Ontology Consortium.* Nat Genet, 2000. 25(1): p. 25-9.

26. Marbach, D., et al., *Tissue-specific regulatory circuits reveal variable modular perturbations across complex diseases.* Nat Methods, 2016. 13(4): p. 366-70.

27. Locke, A.E., et al., *Genetic studies of body mass index yield new insights for obesity biology.* Nature, 2015. 518(7538): p. 197-206.

28. Shungin, D., et al., *New genetic loci link adipose and insulin biology to body fat distribution.* Nature, 2015. 518(7538): p. 187-196.

29. Fuchsberger, C., et al., *The genetic architecture of type 2 diabetes.* Nature, 2016. 536(7614): p. 41-47.

30. Nikpay, M., et al., *A comprehensive 1,000 Genomes-based genome-wide association meta-analysis of coronary artery disease.* Nat Genet, 2015. 47(10): p. 1121-1130.

31. Soranzo, N., et al., *Common variants at 10 genomic loci influence hemoglobin A(1)(C) levels via glycemic and nonglycemic pathways.* Diabetes, 2010. 59(12): p. 3229-39.

32. Manning, A.K., et al., *A genome-wide approach accounting for body mass index identifies genetic variants influencing fasting glycemic traits and insulin resistance.* Nat Genet, 2012. 44(6): p. 659-69.

33. Dupuis, J., et al., *New genetic loci implicated in fasting glucose homeostasis and their impact on type 2 diabetes risk.* Nat Genet, 2010. 42(2): p. 105-16.

34. Willer, C.J., et al., *Discovery and refinement of loci associated with lipid levels.* Nat Genet, 2013. 45(11): p. 1274-1283.

35. Shu, L., et al., *Mergeomics: multidimensional data integration to identify pathogenic perturbations to biological systems.* BMC Genomics, 2016. 17(1): p. 874.

36. Chella Krishnan, K., et al., *Integration of Multi-omics Data from Mouse Diversity Panel Highlights Mitochondrial Dysfunction in Non-alcoholic Fatty Liver Disease.* Cell Syst, 2018. 6(1): p. 103-115 e7.

37. Meng, Q., et al., *Systems Nutrigenomics Reveals Brain Gene Networks Linking Metabolic and Brain Disorders.* EBioMedicine, 2016. 7: p. 157-66.

38. Meng, Q., et al., *Traumatic Brain Injury Induces Genome-Wide Transcriptomic, Methylomic, and Network Perturbations in Brain and Blood Predicting Neurological Disorders.* EBioMedicine, 2017. 16: p. 184-194.

39. Shu, L., et al., *Shared genetic regulatory networks for cardiovascular disease and type 2 diabetes in multiple populations of diverse ethnicities in the United States.* PLoS Genet, 2017. 13(9): p. e1007040.

40. Ntambi, J.M., et al., *Loss of stearoyl-CoA desaturase-1 function protects mice against adiposity.* Proc Natl Acad Sci U S A, 2002. 99(17): p. 11482-6.

41. Ueno, H., et al., *Receptor for advanced glycation end-products (RAGE) regulation of adiposity and adiponectin is associated with atherogenesis in apoE-deficient mouse.* Atherosclerosis, 2010. 211(2): p. 431-6.

42. Yamamoto, Y. and H. Yamamoto, *RAGE-Mediated Inflammation, Type 2 Diabetes, and Diabetic Vascular Complication.* Front Endocrinol (Lausanne), 2013. 4: p. 105.

43. Yan, S.F., R. Ramasamy, and A.M. Schmidt, *The receptor for advanced glycation endproducts (RAGE) and cardiovascular disease.* Expert Rev Mol Med, 2009. 11: p. e9.

44. Eisenstein, A. and K. Ravid, *G protein-coupled receptors and adipogenesis: a focus on adenosine receptors.* J Cell Physiol, 2014. 229(4): p. 414-21.

45. Erion, D.M. and G.I. Shulman, *Diacylglycerol-mediated insulin resistance.* Nat Med, 2010. 16(4): p. 400-2.

46. Rieusset, J., et al., *Suppressor of cytokine signaling 3 expression and insulin resistance in skeletal muscle of obese and type 2 diabetic patients.* Diabetes, 2004. 53(9): p. 2232-41.

47. Samuel, V.T. and G.I. Shulman, *The pathogenesis of insulin resistance: integrating signaling pathways and substrate flux.* J Clin Invest, 2016. 126(1): p. 12-22.

48. He, M., et al., *Induction of HO-1 and redox signaling in endothelial cells by advanced glycation end products: a role for Nrf2 in vascular protection in diabetes.* Nutr Metab Cardiovasc Dis, 2011. 21(4): p. 277-85.

49. Ambele, M.A. and M.S. Pepper, *Identification of transcription factors potentially involved in human adipogenesis in vitro.* Mol Genet Genomic Med, 2017. 5(3): p. 210-222.

50. Jang, M.K. and M.H. Jung, *ATF3 represses PPARgamma expression and inhibits adipocyte differentiation.* Biochem Biophys Res Commun, 2014. 454(1): p. 58-64.

51. Bou, M., et al., *Gene expression profile during proliferation and differentiation of rainbow trout adipocyte precursor cells.* BMC Genomics, 2017. 18(1): p. 347.

52. Li, J.Z., et al., *Circadian patterns of gene expression in the human brain and disruption in major depressive disorder.* Proc Natl Acad Sci U S A, 2013. 110(24): p. 9950-5.

53. Lu, H., et al., *TFEB inhibits endothelial cell inflammation and reduces atherosclerosis.* Sci Signal, 2017. 10(464).

54. Zhao, Q., et al., *TCF21 and AP-1 interact through epigenetic modifications to regulate coronary artery disease gene expression.* Genome Med, 2019. 11(1): p. 23.

55. Costa, R.H., et al., *Transcription factors in liver development, differentiation, and regeneration.* Hepatology, 2003. 38(6): p. 1331-47.

56. Wuschke, S., et al., *A meta-analysis of quantitative trait loci associated with body weight and adiposity in mice.* Int J Obes (Lond), 2007. 31(5): p. 829-41.

57. Wortmann, M., et al., *A Glyoxalase-1 Knockdown Does Not Have Major Short Term Effects on Energy Expenditure and Atherosclerosis in Mice.* J Diabetes Res, 2016. 2016: p. 2981639.

58. Ahmadian, M., et al., *PPARgamma signaling and metabolism: the good, the bad and the future.* Nat Med, 2013. 19(5): p. 557-66.

59. Mariman, E.C. and P. Wang, *Adipocyte extracellular matrix composition, dynamics and role in obesity.* Cell Mol Life Sci, 2010. 67(8): p. 1277-92.

60. Goldberg, I.J. and K.E. Bornfeldt, *Lipids and the endothelium: bidirectional interactions.* Curr Atheroscler Rep, 2013. 15(11): p. 365.

61. Jerome, W.G., *Lysosomes, cholesterol and atherosclerosis.* Clin Lipidol, 2010. 5(6): p. 853-865.

62. Steffens, S., et al., *Circadian Control of Inflammatory Processes in Atherosclerosis and Its Complications.* Arterioscler Thromb Vasc Biol, 2017. 37(6): p. 1022-1028.

63. Nagao, M., et al., *Coronary Disease-Associated Gene TCF21 Inhibits Smooth Muscle Cell Differentiation by Blocking the Myocardin-Serum Response Factor Pathway.* Circ Res, 2020. 126(4): p. 517-529.

64. Sazonova, O., et al., *Characterization of TCF21 Downstream Target Regions Identifies a Transcriptional Network Linking Multiple Independent Coronary Artery Disease Loci.* PLoS Genet, 2015. 11(5): p. e1005202.

65. Geoffrion, M., et al., *Differential effects of glyoxalase 1 overexpression on diabetic atherosclerosis and renal dysfunction in streptozotocin-treated, apolipoprotein E-deficient mice.* Physiol Rep, 2014. 2(6).

66. Jo-Watanabe, A., et al., *Glyoxalase I reduces glycative and oxidative stress and prevents age-related endothelial dysfunction through modulation of endothelial nitric oxide synthase phosphorylation.* Aging Cell, 2014. 13(3): p. 519-28.

67. Yin, W., et al., *Plasma lipid profiling across species for the identification of optimal animal models of human dyslipidemia.* J Lipid Res, 2012. 53(1): p. 51-65.